Acta Pharmaceutica Sinica B 2024;14(10):4360–4377

Chinese Pharmaceutical Association
Institute of Materia Medica, Chinese Academy of Medical Sciences

Acta Pharmaceutica Sinica B

www.elsevier.com/locate/apsb
www.sciencedirect.com

ORIGINAL ARTICLE

Macrophage $P2Y_6R$ activation aggravates psoriatic inflammation through IL-27-mediated Th1 responses

Li Yin [a], Enming Zhang [a], Tianqi Mao [b], Yifan Zhu [b], Shurui Ni [a], Yehong Li [a], Chunxiao Liu [a], Yafei Fang [a], Kexin Ni [a], Yuhe Lu [a], Huanqiu Li [b,*], Mengze Zhou [a,*], Qinghua Hu [a,c,*]

[a]*School of Pharmacy, China Pharmaceutical University, Nanjing 211198, China*
[b]*College of Pharmaceutical Sciences, Soochow University, Suzhou 215006, China*
[c]*School of Life Science and Technology, China Pharmaceutical University, Nanjing 211198, China*

Received 1 March 2024; received in revised form 7 May 2024; accepted 11 June 2024

KEY WORDS

Macrophages;
$P2Y_6R$;
Psoriasis;
FS-6;
IL-27

Abstract Purinergic signaling plays a causal role in the modulation of immune inflammatory response in the course of psoriasis, but its regulatory mechanism remains unclear. As a member of purinoceptors, $P2Y_6R$ mainly distributed in macrophages was significantly up-expressed in skin lesions from patients with psoriasis in the present study. Here, the severity of psoriasis was alleviated in imiquimod-treated mice with macrophages conditional knockout of $P2Y_6R$, while the cell-chat algorithm showed there was a correlation between macrophage $P2Y_6R$ and Th1 cells mediated by IL-27. Mechanistically, $P2Y_6R$ enhanced PLC_β/p-PKC/MAPK activation to induce IL-27 release dependently, which subsequently regulated the differentiation of Th1 cells, leading to erythematous and scaly plaques of psoriasis. Interestingly, we developed a novel $P2Y_6R$ inhibitor FS-6, which bonds with the ARG266 side chain of $P2Y_6R$, exhibited remarkable anti-psoriasis effects targeting $P2Y_6R$. Our study provides insights into the role of $P2Y_6R$ in the pathogenesis of psoriasis and suggests its potential as a target for the development of therapeutic interventions. A novel $P2Y_6R$ inhibitor FS-6 could be developed as an anti-psoriasis drug candidate for the clinic.

*Corresponding authors.
E-mail addresses: huanqiuli@suda.edu.cn (Huanqiu Li), zmz@cpu.edu.cn (Mengze Zhou), huqh@cpu.edu.cn (Qinghua Hu).

Peer review under the responsibility of Chinese Pharmaceutical Association and Institute of Materia Medica, Chinese Academy of Medical Sciences.

https://doi.org/10.1016/j.apsb.2024.06.008

1. Introduction

Psoriasis is an immune-mediated, genetic disease and is characterized by erythematous and scaly plaques of the skin. It affects approximately 1.5% of the global population[1]. Histologically, psoriatic lesions are characterized by the activation of numerous immune cells infiltrating into the dermis[2-4]. Purine metabolism plays a crucial role in the pathogenesis of psoriasis, which is associated in the development and progression of this chronic inflammatory skin disorder[5,6]. In the progression of psoriasis, UDP has to be necessarily released extracellularly by damaged cells[7]. Once in the extracellular milieu, this nucleotide may play different roles both by inducing chemotaxis of immune cells and by amplifying the inflammatory response[6,8]. More importantly, modulation of purinergic signaling regulates many skin functions, including keratinocyte proliferation, skin repair, and immune response, particularly in inflammasome activation[8,9]. Thus, targeting single molecular actors of the purinoceptors may develop new psoriasis treatments.

In the present study, we analyzed gene expression from psoriasis patient skin samples and found that $P2Y_6R$ played a significant role in the progression of psoriasis. To further investigate the mechanisms of $P2Y_6R$, we examined the spatial localization and expression profile of $P2Y_6R$ and generated mice with conditional knockout of $P2Y_6R$ in macrophages. Our results demonstrated that macrophage $P2Y_6R$ mediated PLC_β/p-PKC/MAPK signaling, enhanced skin inflammation by the release of IL-27, which led to increased Th1 cell differentiation and amplified IFN-γ-mediated skin inflammation *via* the IL-27RA mediated p-JAK2/p-STAT1/T-bet signaling pathway. Additionally, we sought to identify a potent $P2Y_6R$ inhibitor that could have a direct therapeutic effect on psoriasis. These findings offer a potential treatment strategy for psoriasis through $P2Y_6R$-targeted therapy.

2. Materials and methods

2.1. Cells

HEK293-h$P2Y_6R$ cells obtained from KeyGEN Biotech (Jiangsu, China, KG345) were cultured in DMEM (KGM12800N-500, KeyGEN, Jiangsu, China) supplemented with 10% FBS (FBSSA500-5, AusGeneX, Shanghai, China), 100 units/mL penicillin, 100 μg/mL streptomycin, and 2 mol/L L-glutamine in a humidified atmosphere of 5% CO_2 at 37 °C.

BMDMs were derived from bone marrow cells isolated from mice femurs and tibias and cultured in DMEM medium (11965092, Gibco, NY, USA) containing 10% FBS (FBSSA500-5, AusGeneX, Shanghai, China), 1% penicillin-streptomycin, and 20% (*v*/*v*) L-929 cell-conditioned medium to promote macrophage colony growth. The adherent cells were used for experiments after 7 days of culture at 37 °C under 5% CO_2. BMDMs were extracted and seeded in 24-well plates. After 24 h, 10 μmol/L UDP (BCCB4639, Sigma−Aldrich, Germany) was added for model stimulation; 30 min later, 4 ng/mL IMQ (HY-B0180, MedChemExpress, New Jersey, USA) was added, 12 h later, the supernatant was collected and IL-27 concentration was measured. For IL-27 reverse experiments, BMDMs were stimulated with 100 nmol/L PMA (HY-18739), 5 nmol/L Anisomycin (HY-18982), 20 μmol/L Cigilitazone (HY-W011220) and 10 μmol/L Ceramide C6 (HY-19542, all from MedChemExpress) for 12 h before UDP and IMQ treatment.

Naïve T cells were isolated from the spleens of adult mice using standard protocols. Mice were euthanized and the spleens were dissected. After washing the spleen three times in PBS containing 5% FBS, the cells were filtered through a 70 μm cell strainer to obtain a cell suspension. Following red blood cell lysis, using CD4 magnetic beads (551539, BD Biosciences, New Jersey, USA) to isolate CD4-positive T cells. Subsequently, cells were seeded in a 12-well plate pre-coated with anti-mouse CD3e (BE0001-1-1MG, Bioxcell, New Hampshire, USA). For Th1 cells polarization, 10 ng/mL IL-12 (HY-P70666) and 10 μg/mL anti-IL-4 (HY-P990121, both from MedChemExpress, New Jersey, USA) were added into IMDM complete culture medium (KGM12200-500, KeyGEN, Jiangsu, China). The cells were incubated at 37 °C in a humidified incubator with 5% CO_2 for 5 days. After 5 days of culture, Th1 cells were stimulated with 50 ng/mL PMA (TQ0198, Topscience, Shanghai, China), 500 ng/mL ionomycin (HY-13434), and 10 μg/mL brefeldin A (HY-16592, both from MedChemExpress) incubated for 4.5 h at 37 °C for subsequent flow cytometry analysis. Purified naive CD4 T-cells were cultured with the supernatants from BMDMs at a 1:1 ratio, in the presence of plate-coated α-CD3 (BE0001-1-1MG)/CD28 (BE0015-1-1MG, both from Bioxcell, New Hampshire, USA) antibodies at a concentration of 1 μg/mL, for 3 days. The IFN-γ^+CD4$^+$T-cells were detected by FACS.

2.2. Mice

The $P2Y_6R$ deficient mice ($P2Y_6R^{-/-}$) mice in C57BL/6J background were obtained from GemPharmatech Co., Ltd. (Strain No. T052843, Jiangsu, China). $P2Y_6R$-floxed ($P2Y_6R^{fl/fl}$) mice were generated at GenPharmatech Co., Ltd. *Lyz2*$^{-Cre}$ mice (B6. 129P2-Lyz2tm1(cre)Ifo/J; stock No. 04781) were purchased from Jackson Laboratory (Bar Harbor, ME). IL-27ra$^{-/-}$ mice were given by Assoc. Prof. Qian Wang, (Jinan University, Guangzhou, China) and CD4^{-cre} mice were kindly donated by Prof. Xinming Jia (Shanghai Tenth People's Hospital, School of Medicine, Tongji University, Shanghai, China).

All mice were housed in a controlled environment (20 ± 2 °C, 12-h/12-h light/dark cycle), where they were maintained on a standard chow diet with free access to water. The genotypes of the mice were examined *via* PCR using the total DNA derived from the tail tips (Supporting Information Fig. S1). The primers used are listed in Supporting Information Table S1. The experimental animal facility has been accredited by the Association for Assessment and Accreditation of Laboratory Animal Care International (AAALAC). All mouse experiments conformed to the NIH guidelines (Guide for the Care and Use of Laboratory Animals), and the ethical approvals for the animal experiments were obtained from the Animal Ethics Committee of China Pharmaceutical University (No. AECCPU201902004).

2.3. In vivo experiments

IMQ-induced psoriasis-like skin inflammation was induced by a daily topical dose of 62.5 mg of IMQ cream (5%) (Sichuan MedShine Pharmaceutical Co., Sichuan, China) on the shaved back for five consecutive days. One day before the initiation of experiments, mice were shaved along their upper backs using electric clippers. On the indicated days, the skin thickness was measured

with a micrometer. In the IL-27 revertant experiments, a subcutaneous administration of either IL-27 recombinant protein (RP00702, Abclonal, Wuhan, China) or saline was conducted at a dosage of 400 ng per day. In the treatment of $P2Y_6R$ inhibitor, FS-6 (at a dosage of either 10 or 20 mg/kg) MTX (at a dosage of 1 mg/kg) was administered *via* intraperitoneal injection on a daily basis prior to the application of IMQ. The treatment regimen was continued until the completion of the model establishment process.

2.4. Histology, IF and IHC staining

Tissue samples from the dorsal skin were harvested, 4% paraformaldehyde-fixed, and paraffin-embedded. Sections were stained with hematoxylin and eosin stain for histological analysis. For immunofluorescence, sections of mouse skin were stained with anti-mouse CD86 (ab239075, Abcam, Cambridge, UK) or anti-mouse $P2Y_6R$ primary antibody (DF6956, Affinity, Jiangsu, China), followed by Alexa Fluor 488−conjugated secondary antibody (ab150113, Abcam). The expression of Ki67 in the skin was detected by immunohistochemistry. Antigen retrieval was carried out by boiling the sections in sodium citrate solution (pH = 6.0). The sections were washed and blocked with 3% hydrogen peroxide to inhibit endogenous peroxidase. Then, the sections were incubated with a Ki67 primary antibody (ab15580, Abcam) overnight. The following day, the sections were washed with PBS and incubated with a secondary antibody at room. Images were captured using BX53 biological microscope (OLYMPUS) and analyzed by ImageJ software.

2.5. RNA extraction and real-time quantitative PCR

Total RNA was isolated from skin biopsies using RNA isolater Total RNA Extraction Reagent (R401-01, Vazyme, Jiangsu, China). Total RNA was used to prepare cDNA using the HiScript II Q RT SuperMix for qPCR (+gDNA wiper) (R222-01, Vazyme). Real-time PCR was carried out using SYBR Green (AQ602-01, TransGen Biotech, Jiangsu, China) endpoint measurement. Expression was calculated using the ΔC_T method relative to the housekeeping gene *GAPDH*. Primer sequences are provided in Supporting Information Table S2.

2.6. Flow cytometry

Back skin was cut into small pieces and digested in RPMI−2% fetal calf serum (FCS) supplemented with 1 mg/mL collagenase IV (C4-28-100 MG, Sigma−Aldrich, Missouri, USA) and 100 μg/mL deoxyribonuclease (DNase) I (10104159001, Sigma−Aldrich, Missouri, USA) at 37 °C for 1.5 h. After digestion, the skin tissue was disrupted with a syringe with an 18-gauge needle, filtered through a 70-μm cell strainer, and washed with PBS. Then cells were stained with fluorophore-conjugated antibodies: CD4-FITC (11-0042-85, Invitrogen, CA, USA), CD11c-PE-cy7 (25-0114-82, Invitrogen, California, USA), CD86-FITC (11-0862-82, Invitrogen), NK1.1-PE (12-5941-82, Invitrogen), IFN-γ-PE (12-7311-82, Invitrogen), IL-17A-APC (17-7177-81, Invitrogen), CD45-PE-Cy7 (25-0451-82, Invitrogen), CD207,-Alexa Flour 488 (53-2073-82, Invitrogen), CD163-PE (12-1631-82, California, USA), MHCII-Percp-cy5.5 (562363, BD Pharmingen, New Jersey, USA). After washing, the cells were assayed with a BD FACS Celesta flow cytometer, and the data were analyzed using FlowJo software.

2.7. Immunoblotting

Cells and skin tissues were lysed for immunoblotting in radioimmunoprecipitation assay (RIPA) buffer (P0013B, Beyotime, Shanghai, China) containing PMSF (ST506, Beyotime, Shanghai, China) and phosphatase inhibitors (P1082, Beyotime) at the indicated time points. The following antibodies were used: PLC_β (bs-6976R, Bioss, Beijing, China), PKC (ab181558, Abcam, Cambridge, UK), p-PKC (EP2730Y, Abcam), p38 (AF6456, Affinity, Jiangsu, China), p-p38 (AF4001, Affinity), ERK (bs-0022R, Bioss), p-ERK (bs-3016R, Bioss), p-JAK2 (A19629, Abclonal, Wuhan, China), JAK2 (AP0531, Abclonal), p-STAT1 (bs1657R, Bioss), STAT1 (10144-2-AP, Proteintech, Wuhan, China), p-JNK (bs1640R, Bioss), JNK (AF6318, Affinity), T-bet (14-5825-82, Abclonal), β-actin (T0022, Affinity).

2.8. Enzyme-linked immunosorbent assay (ELISA)

Supernatants of cell culture, mice serum and skin were collected and stored in −70 °C freezer[14]. IL-27 and IFNγ were detected by mouse IL-27 ELISA kit (EMC115.96, Neobioscience Technology, Shenzhen, China) and mouse IFNγ ELISA kit (EK280HS, MULTI Sciences, Hangzhou, China) according to the manufacturer's instructions.

2.9. Transfection

Cells were seeded in 6 well plates, and grown to 80% confluence prior to infection. Plasmid (SinoBiological, Beijing, China) were added with diluted Lipofectamine™ 3000 reagent (L3000001, Invitrogen, California, USA) in Opti-MEM™ Medium (31985070, Gibco, CA, USA) according to the manufacturer's instructions. The medium was replaced with fresh medium 6 h after transfection. Cells were cultured for 48 h before treatment with the indicated agents.

2.10. Grating-coupled interferometry (GCI)

$P2Y_6R$ was immobilized on a 4PCP WAVE chip by standard amine coupling chemistry with a flow of 10 μL/min to the desired surface density level. An empty surface was activated/deactivated and used as a reference channel. Throughout all experiments, the running buffer was the PBS-P buffer and 3% DMSO at pH 7.5 (all reagents from Sigma). The kinetic run (all at 60 μL/min) included 20 startup cycles of running buffer injections followed by a 1:2 dilution series of compound FS-6 (eight concentrations, with 100 μmol/L as the highest concentration) with one blank every injection. DMSO calibrations were performed at the end of the series. All the cycles in the kinetic run included 45 s baseline, 60 s association, and 60 s dissociation. No regeneration was required.

Data adjustments and analysis were performed with the Creoptix WAVE control software. Adjustments included DMSO calibration correction, X-offset correction, and blank subtraction using the closest blank. Global fitting with bulk correction for both association and dissociation was used to obtain the kinetic rate constants K_D and R_{max}. Equilibrium analysis included an offset correction.

2.11. Cellular thermal shift assay (CETSA)

CETSA was performed in accordance with a previous study. Briefly, The HEK293-h$P2Y_6R$ cells were divided into two groups.

The collected HEK293-hP2Y$_6$R cells were incubated with FS-6 for 30 min. Each group was divided into six equal parts and heat-treated at different temperatures for 10 min. Then, the samples were quickly transferred to ice and centrifuged at 12,000 rpm with a cryogenic centrifuge for 10 min. The supernatants were obtained, added with loading buffer, and analyzed using Western blot.

2.12. GSEA, GO, and KEGG analysis

The GEO datasets were acquired from https://www.ncbi.nlm.nih.gov/geo and the analysis was conducted using Rstudio (Version 4.3.1). The identification of differentially expressed genes utilized the GO and KEGG pathway enrichment analyses, available at https://david.ncifcrf.gov. The GSEA analysis was performed using GSEA v3.0 at http://www.broadinstitute.org/gsea/.

2.13. Protein−protein interaction network

The STRING database was used to identify the protein−protein interaction (PPI) networks of differentially expressed genes.

2.14. Single-cell RNA seq analysis

The analysis was conducted following the standard procedure outlined in Seurat v3. In the cell quality control (QC) step, cells that expressed less than 200 genes or greater than 7500 genes were excluded, as well as those with more than 5% erythrocyte genes or more than 20% mitochondrial genes. After normalization and principal component analysis (PCA) dimension reduction, cell clustering was performed based on PCA dimensionality reduction using the first 20 principal components and a resolution value of 0.4. For cell annotation, marker genes were manually identified with the assistance of the CellMarker 2.0 database available at http://bio-bigdata.hrbmu.edu.cn/CellMarker. The marker genes for each cluster were determined using the FindAllMarkers function with default parameters.

2.15. Cibersort

CIBERSORT v2.0 was employed for cell type analysis in this study. A reference gene expression profile was obtained from publicly available gene expression datasets, which contained data from multiple known cell types. The reference gene expression profile was then compared with the sample gene expression datasets. To accurately infer the cell type composition, a linear regression model was utilized, and the sample gene expression data was fitted to the reference gene expression profile using the least squares method. In this model, consideration was given to the batch effects of the gene expression data, and necessary corrections were performed.

2.16. Cellchat

Cell−cell communication analysis was conducted on a single-cell RNA sequencing dataset using the CellChat R package. Ligand−receptor interactions were identified and quantified for each pair of cell types. Intercellular communication relied on the inferred ligand and receptor profiles, where the expression levels of ligands and receptors were estimated by calculating the geometric mean across individual cells of a specific cell type. These interactions indicate the strengths of interactions between all ligands and their corresponding receptors expressed in the two specified cell types.

2.17. Transcription factor enrichment analysis

ChEA3 (https://amp.pharm.mssm.edu/ChEA3) was used to find and annotate the main biological functions of the TF targets involved in sample gene expression datasets.

2.18. Chemistry

All reagents and solvents were commercially available and were used without further purification. Varian UNITY INOVA 400 and 600 MHz NMR instruments were used to determine the hydrogen and carbon spectra of NMR. TMS was the internal standard at 25 °C. The ESI-MS spectra were recorded on a Xevo G2-XS TOF mass spectrometer. The EI-MS spectra were recorded on a GCT Premier mass spectrometer. The silica gel used for the separation of compound column chromatography (CC) was a 200−300 mesh column chromatography silica gel produced by Qingdao Ocean Chemical Works. The amount of silica gel was 50−100 times the amount of separated samples. The whole elution process was tracked by thin layer chromatography (TLC). The silica gel 60 GF254 produced by Qingdao Ocean Chemical Works was used for thin layer chromatography. The silica gel 60 GF254 was detected by ultraviolet radiation at 254 nm wavelength. The purity of the compound was, analyzed by HPLC (Agilent 1100 Series; Multohyp ODS-5μ, 4.6 mm × 250 mm), and the final compounds exhibited purity greater than 95%. The applied mobile phases were 95% MeOH/5% H_2O. The flow speed was 1.2 mL/min, and injection volumes were 10 or 20 μL. Melting points were determined with Shanghai Jingke Industrial X-4A11 and are uncorrected.

2.19. Molecular dynamics (MD) simulations

The dynamic interaction patterns between compounds A6, FS-6, and P2Y$_6$R were investigated by the MD simulations[29]. The general AMBER force field (gaff) and the ff99SBildn force field[18] were used for the two compounds and P2Y$_6$R, respectively. Each compound was optimized by Gaussian 09 at the HF/6-31G* level, and then the atomic partial charges were obtained by fitting the electrostatic potentials using the RESP fitting technique in Amber. The system was neutralized with the counter ions of Na^+. The whole system was immersed in a rectangular box of TIP3P water molecules[17], and the water box was extended Å from any solute atom. The particle mesh Ewald (PME) method was employed for the long-range electrostatics.

Each system was relaxed by a two-stage minimization protocol: first, the protein was fixed, and the water molecules and ligand were minimized by 500 cycles of steepest descent and 500 cycles of conjugate gradient minimization; second, the whole system was minimized by 5000 cycles (1000 cycles of steepest descent and 4000 cycles of conjugate gradient minimization). Then, 10 ns MD simulation was performed under a target temperature of 300 K and a target pressure of 1 atm. The SHAKE procedure was employed to constrain all bonds involving hydrogen atoms, and the time step was set to 2 fs. Coordinate trajectories were saved every 10 ps. The MM simulations and MD optimizations were accomplished by using the sander program in AMBER11.

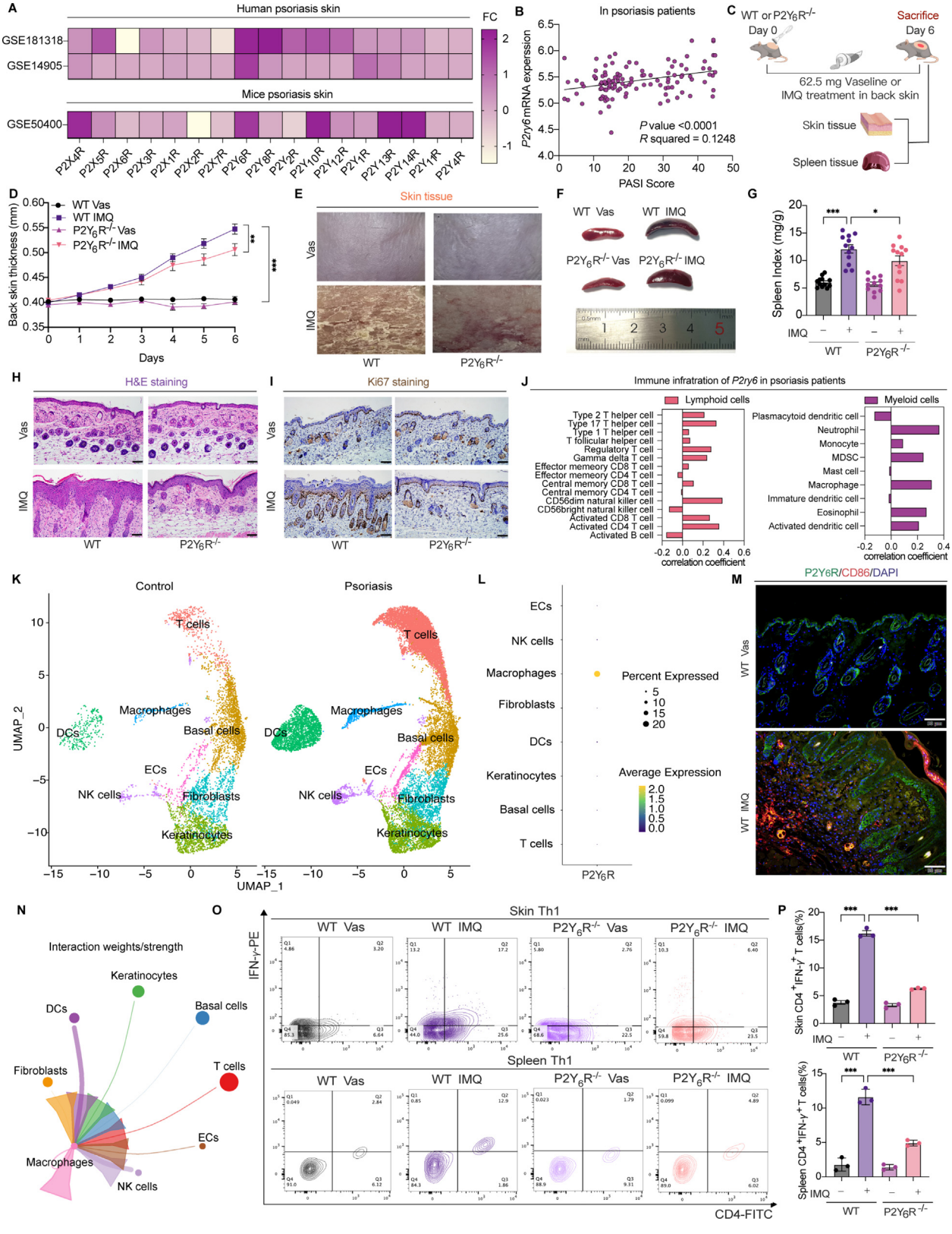
A
Human psoriasis skin
GSE181318
GSE14905
Mice psoriasis skin
GSE50400
FC
P2X4R P2X5R P2X6R P2X3R P2X1R P2X2R P2X7R P2Y6R P2Y8R P2Y2R P2Y10R P2Y12R P2Y1R P2Y13R P2Y14R P2Y11R P2Y4R
B
In psoriasis patients
P2ry6 mRNA experssion
P value <0.0001
R squared = 0.1248
PASI Score
C
WT or P2Y6R-/-
Day 0
Sacrifice
Day 6
62.5 mg Vaseline or
IMQ treatment in back skin
Skin tissue
Spleen tissue
D
WT Vas
WT IMQ
P2Y6R-/- Vas
P2Y6R-/- IMQ
Back skin thickness (mm)
Days
E
Skin tissue
Vas
IMQ
WT
P2Y6R-/-
F
WT Vas
WT IMQ
P2Y6R-/- Vas
P2Y6R-/- IMQ
G
Spleen Index (mg/g)
IMQ
WT
P2Y6R-/-
H
H&E staining
I
Ki67 staining
J
Immune infratration of P2ry6 in psoriasis patients
Lymphoid cells
Type 2 T helper cell
Type 17 T helper cell
Type 1 T helper cell
T follicular helper cell
Regulatory T cell
Gamma delta T cell
Effector memeory CD8 T cell
Effector memeory CD4 T cell
Central memory CD8 T cell
Central memory CD4 T cell
CD56dim natural killer cell
CD56bright natural killer cell
Activated CD8 T cell
Activated CD4 T cell
Activated B cell
correlation coefficient
Myeloid cells
Plasmacytoid dendritic cell
Neutrophil
Monocyte
MDSC
Mast cell
Macrophage
Immature dendritic cell
Eosinophil
Activated dendritic cell
correlation coefficient
K
Control
Psoriasis
T cells
Macrophages
DCs
Basal cells
ECs
NK cells
Fibroblasts
Keratinocytes
UMAP_1
UMAP_2
L
ECs
NK cells
Macrophages
Fibroblasts
DCs
Keratinocytes
Basal cells
T cells
P2Y6R
Percent Expressed
Average Expression
M
P2Y6R/CD86/DAPI
WT Vas
WT IMQ
N
Interaction weights/strength
Keratinocytes
DCs
Basal cells
Fibroblasts
T cells
ECs
Macrophages
NK cells
O
Skin Th1
Spleen Th1
WT Vas
WT IMQ
P2Y6R-/- Vas
P2Y6R-/- IMQ
IFN-γ-PE
CD4-FITC
P
Skin CD4+IFN-γ+T cells(%)
Spleen CD4+IFN-γ+T cells(%)
IMQ
WT
P2Y6R-/-

2.20. MM/GBSA binding free energy calculations/ decompositions

The binding free energy (ΔG_{bind}) of each compound/P2Y$_6$R was calculated by the Molecular Mechanics/Generalized Born Solvent Area (MM/GBSA) methodology[29,30] as in Eq. (1):

$$\begin{aligned}\Delta G_{bind} &= G_{complex} - G_{protein} - G_{ligand} \\ &= \Delta H + \Delta G_{solvation} - T\Delta G \\ &= \Delta E_{MM} + \Delta G_{GB} + \Delta G_{SA} - T\Delta S \end{aligned} \quad (1)$$

where ΔE_{MM} represents the gas-phase interaction energy between the protein and ligand, which contains the electrostatic (ΔE_{ele}) and van der Waals (ΔE_{vdw}) terms, and ΔG_{GB} and ΔG_{SA} are the polar entropy ($-T\Delta S$) were not considered because of the high computational cost and low prediction accuracy. The electrostatic solvation energy (ΔG_{GB}) was calculated by using the GB model with the parameters developed by Onufriev et al.[31] (igb = 2). The exterior dielectric constant was set to 80, and the solute dielectric constant value was set to 1. The nonpolar contribution of desolvation (ΔG_{SA}) was estimated by the solvent-accessible surface area using the LCPO method[32]. All energy components were calculated using 100 snapshots extracted from 2.0 to 10 ns.

The MM/GBSA free energy decomposition in the mm_pbsa program in AMBER11 was employed to analyze the interactions between each residue in P2Y$_6$R and compounds A6 and FS-6. The residue−ligand interaction consists of four parts: van der Waals contribution (ΔG_{vdw}), electrostatic contribution (ΔG_{ele}), the polar part of desolvation (ΔG_{GB}), and the nonpolar part of desolvation (ΔG_{SA}). The exterior dielectric constant was set to 80, and the solute dielectric constant value was set to 1. The nonpolar contribution of desolvation (ΔG_{SA}) was calculated by SASA using the ICOSA technique[33].

2.21. Statistical analysis

GraphPad Prism V.9 (San Diego, CA, USA) was used for statistical analysis. Data are presented as mean ± SEM. Tests used include One-way ANOVA with Tukey multiple comparison test, two-way ANOVA with Sidak's multiple comparisons test, and Unpaired T test. $P < 0.05$ was considered statistically significant. All data are representative of at least three independent experiments.

3. Results

3.1. P2Y$_6$R expression is increased in psoriatic lesional skin and its deficiency alleviates the severity of IMQ-induced psoriasis

To explore the differences between purinergic gene expressions involved in psoriasis progression, we performed a GEO2R analysis. Among all the P2X and P2Y receptor families, P2Y$_6$R level was dramatically up-regulated both in psoriasis skin and psoriasis mouse model (Fig. 1A). Besides, P2Y$_6$R expression was positively correlated with PASI scores in patients with psoriasis (GSE117468) (Fig. 1B). Further analysis comparing the two datasets revealed 110 common DEGs (Supporting Information Fig. S2A−S2D, Table S3). Interestingly, P2Y$_6$R was in the top 30 DEGs in the PPI network (Fig. S2E). Thus, we speculated that P2Y$_6$R played an important regulatory role in psoriasis.

Accordingly, we generated P2Y$_6$R knockout mice (P2Y$_6$R$^{-/-}$) and established an IMQ-induced psoriasis mouse model (Fig. 1C)[10]. It was shown that the PASI scoring, spleen index, and histological analysis showed that the severity of psoriasis was alleviated in the IMQ-treated P2Y$_6$R$^{-/-}$ mice compared to the IMQ-treated WT mice (Fig. 1D−I).

It has been suggested that purinergic receptor signaling networks interacted with immune cell responses[2,3]. To investigate whether P2Y$_6$R alterations were associated with immune infiltrate in psoriasis, we used CIBERSORTX to excavate its functional role in the immune system. Among the 22 immune cell fractions, psoriasis patients exhibited high infiltration levels of CD4$^+$ T cells, Th cells, NK resting cells, M1 macrophages, and activated DCs (Fig. S2F). Specifically, *P2ry6* was found to be highly expressed in M1 macrophages (Fig. 1J). Reanalysis of scRNA-seq of skin from healthy controls and patients with psoriasis also showed up-regulation of *P2ry6* in macrophages from lesional skin in psoriasis patients (Fig. 1K, L and Supporting Information Fig. S3). This observation was validated by the co-localization of P2Y$_6$R with M1 macrophages in the dermis of IMQ-treated WT mice (Fig. 1M). However, despite a more comprehensive PASI analysis showing the psoriasis was alleviated in the IMQ-treated P2Y$_6$R$^{-/-}$ mice (Supporting Information Fig. S4A), the proportion of M1 macrophages did not change significantly after P2Y$_6$R depletion (Fig. S4B). Given the importance of macrophages in mediating cell−cell interactions in psoriasis[2,11,12], it was suggested that macrophages had the potential connection between T cells, NK cells, or DCs in the CELLCHAT algorithm communication network (Fig. 1N).

Figure 1 Macrophage P2Y$_6$R expression is increased in psoriatic lesional skin and involved in Th1 cells mediated psoriasis processes. (A) Expression of purinergic receptors in human and mice psoriasis skin. (B) Linear regression analysis indicated a positive correlation between *P2ry6* mRNA expression and PASI score in GSE117468. (C) Flow diagram. (D) Skin thickness was measured from Day 0 to Day 6 ($n = 12$). (E) Represent images for the psoriatic appearance on IMQ or Vaseline-treated WT mice and P2Y$_6$R$^{-/-}$ mice skin. (F) The representative image of spleen from the mice. (G) The spleen index on Day 6 ($n = 12$). (H) H&E staining of IMQ-treated WT mice and P2Y$_6$R$^{-/-}$ mice skin ($n = 3$). (I) Ki67 staining of skin tissues from WT or P2Y$_6$R$^{-/-}$ mice treated with Vaseline or IMQ ($n = 3$). (J) Immune infiltration correlation coefficient of lymphoid cells and myeloid cells of *P2ry6* in GSE181318 and GSE14905. (K) scRNA-seq data of GSE151177 were grouped into 8 clusters with UMAP. (L) Expression of P2Y$_6$R in different cells form scRNA-seq data. (M) Represent immunofluorescence images of Macrophages CD86 (red) and P2Y$_6$R (green) co-localization in mice skin treated with Vaseline or IMQ ($n = 3$). Scale bar = 50 μm. (N) CellChat analysis indicated the inferred interaction among macrophages in psoriasis patient. (O−P) Th1 cells (CD4$^+$ IFNγ^+) proportion was decreased in IMQ-induced P2Y$_6$R$^{-/-}$ mice skin and spleen ($n = 3$). Data are expressed as mean ± SEM. *$P < 0.05$, **$P < 0.01$, ***$P < 0.001$.

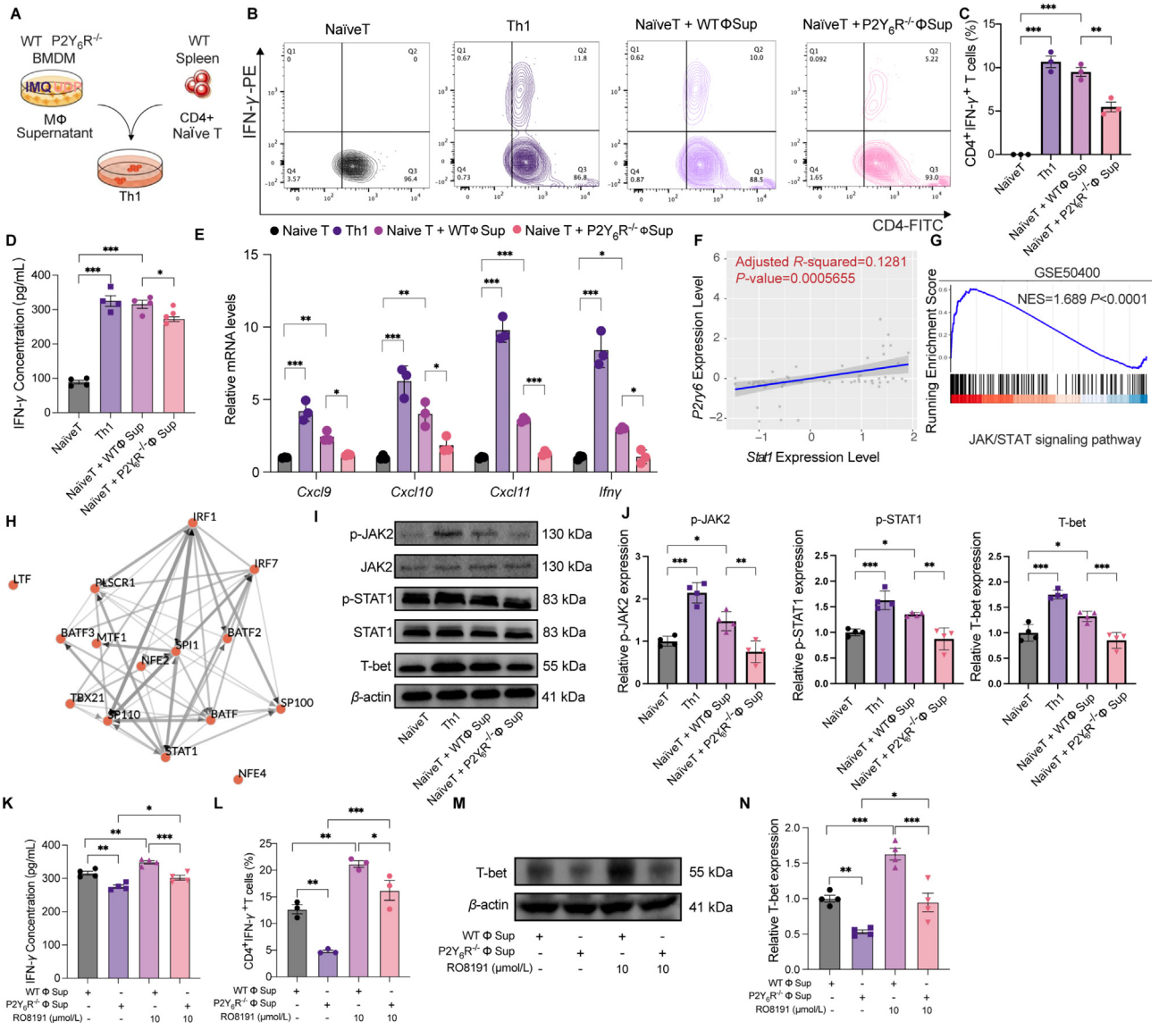

Figure 2 Macrophage P2Y$_6$R mediated Th1 type psoriasis-like inflammation *via* p-JAK2/p-STAT1/T-bet signaling. (A) Flow diagram. (B, C) FACs and the statistical analysis of IFNγ^+ CD4$^+$ T-cells ($n = 3$). (D) IFNγ concentration after WT or P2Y$_6$R$^{-/-}$ mice BMDM supernatant inducing Naïve CD4$^+$ T-cells ($n = 4$). (E) The mRNA expression of the Th1-associated cytokines, *Ifnγ*, *Cxcl9*, *Cxcl10,* and *Cxcl11* were detected by RT-qPCR ($n = 3$). All mRNA levels were normalized to GAPDH. (F) Linear regression analysis indicated a positive correlation between *P2ry6* and *Stat1* in GSE181318 and GSE14905. (G) GSEA analysis of GSE50400 showed JNK/STAT signaling pathways were up-regulated in IMQ-induced mice. (H) Top 15 putative transcription factors based on ChEA3. (I, J) The protein expression levels of p-JAK2, p-STAT1, and T-bet in T cells. Normal protein levels were normalized to β-actin, the values for the phosphorylated forms of proteins were normalized to phosphorylation-independent levels of the same protein ($n = 4$). (K) CD4$^+$ Naïve T cells supernatant IFNγ concentration after WT or P2Y$_6$R$^{-/-}$ mice BMDM supernatant inducing and being treated with or without RO8191 ($n = 4$). (L) The proportion of IFNγ^+ CD4$^+$ T cells of CD4$^+$ Naïve T cells after WT or P2Y$_6$R$^{-/-}$ mice BMDM supernatant inducing and being treated with or without RO8191 ($n = 3$). (M, N) T-bet protein expression of CD4$^+$ Naïve T cells after WT or P2Y$_6$R$^{-/-}$ mice BMDM supernatant inducing and being treated with or without RO8191 ($n = 4$). Data are expressed as mean ± SEM. *$P < 0.05$, **$P < 0.01$, ***$P < 0.001$.

Therefore, we detected immune cell responses in the skin and spleen tissue including Th1 cells, Th17 cells, DCs, and NK cells after P2Y$_6$R depletion. Since the diversity of macrophage populations in psoriasis, we also detected CD163$^+$ M2 macrophage cell percentage after P2Y$_6$R knockout. However, we found there is no significant difference in M2 cell percentage between P2Y$_6$R-deficient mice and WT mice, suggesting that P2Y$_6$R depletion only impaired inflammatory macrophage activation and did not favor the M1 or M2 phenotype. Importantly, compared with IMQ-treated WT mice, Th1 cells were the most significantly decreased (Fig. 1O, P and Fig. S4D–S4F). Besides, to verify whether P2Y$_6$R on Langerhans cells is activated and affects the course of psoriasis, CD45$^+$CD207$^+$MHCII$^+$ LCs were counted both in the epidermis and the dermis. However, we found no difference in the distribution and density of Langerhans cells and CD11c$^+$

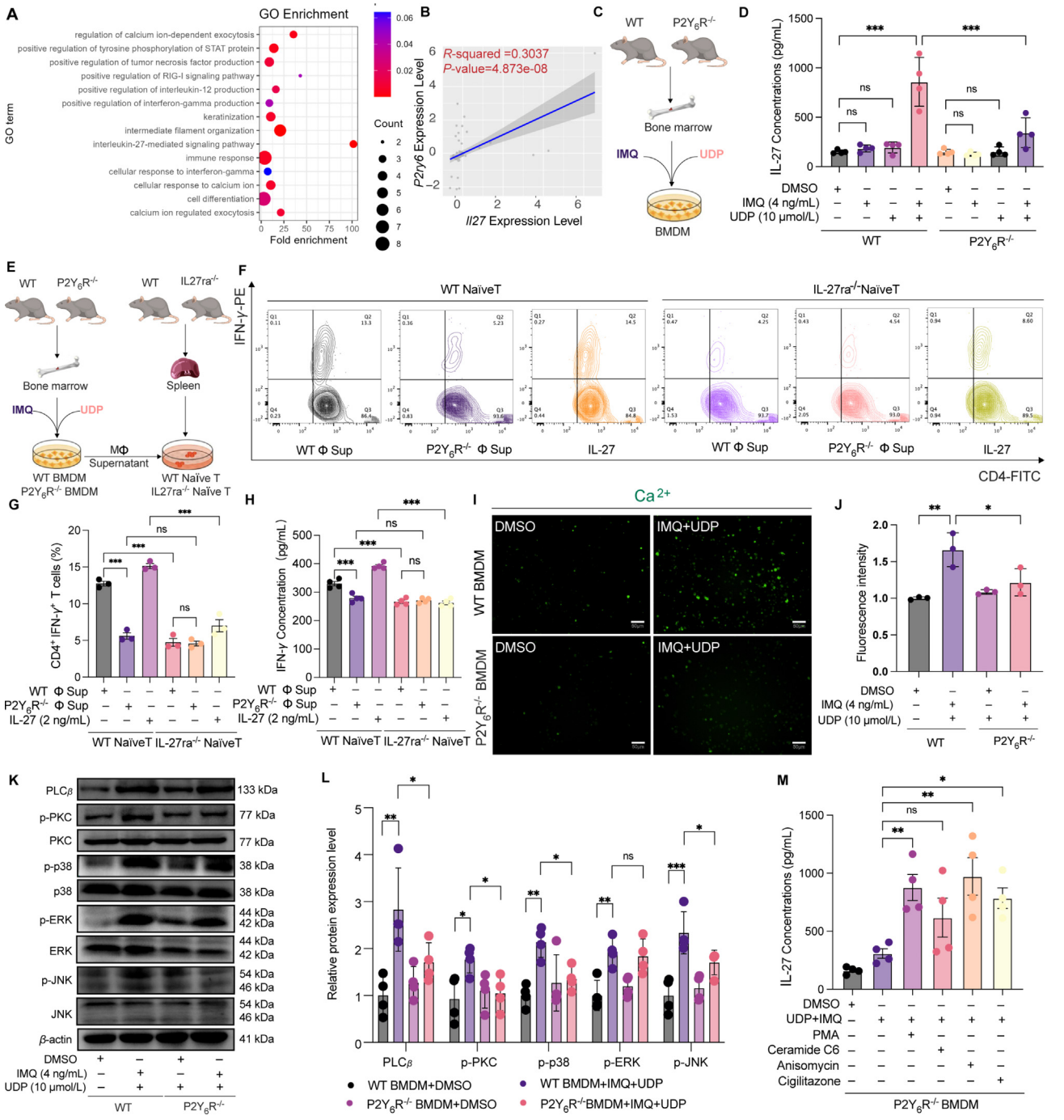

Figure 3 P2Y$_6$R enhances IL-27 released from macrophages. (A) Top15 BPs were shown through GO analysis of DEGs. (B) Linear regression analysis indicated a positive correlation between *P2ry6* and *Il-27* in GSE181318 and GSE14905. (C) Flow diagram. (D) The IL-27 concentration in the supernatants of P2Y$_6$R$^{-/-}$ or WT BMDMs induced by IMQ and UDP ($n = 4$). (E) Flow diagram. (F–G) The proportion of Th1 cells differentiated from IL27ra$^{-/-}$ Naïve T cells has no significant variability between WT BMDMs and P2Y$_6$R$^{-/-}$ BMDMs supernatant stimulation tested by FACs ($n = 3$). (H) WT or IL27ra$^{-/-}$ mice CD4$^+$ Naïve T cells supernatant IFNγ concentration after WT or P2Y$_6$R$^{-/-}$ mice BMDM supernatant inducing ($n = 4$). (I) Changes in BMDMs intracellular Ca^{2+} were measured using the Ca^{2+} detection Fluo-4AM molecular probes. (J) Quantitative analysis of fluorescence intensity. (K–L) Protein expression in different groups. Normal protein levels were normalized to β-actin, the values for the phosphorylated forms of proteins were normaliszd to phosphorylation-independent levels of the same protein ($n = 4$). (M) The IL-27 concentration in the supernatant. Data are expressed as mean ± SEM. $^*P < 0.05$, $^{**}P < 0.01$, $^{***}P < 0.001$.

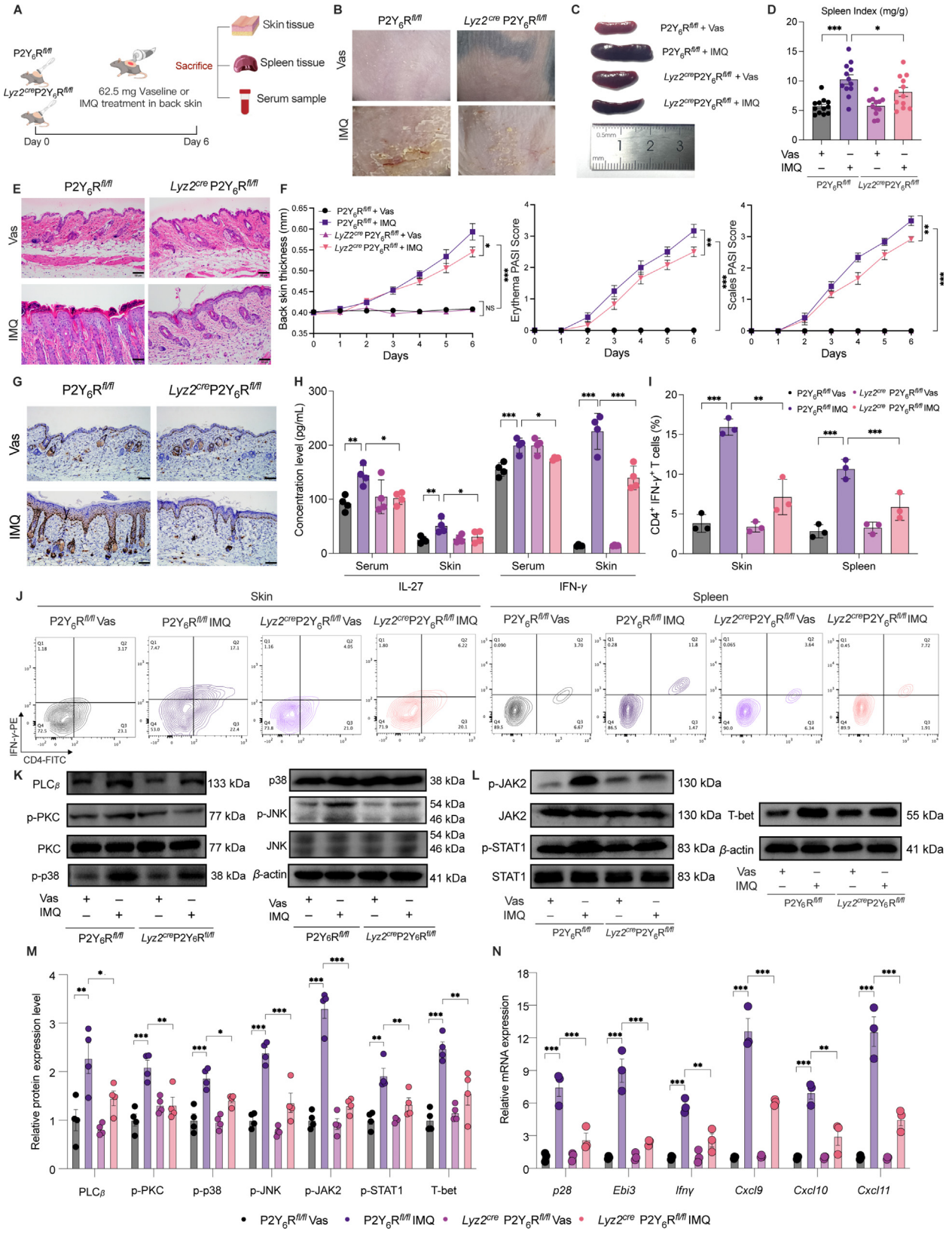
A
Sacrifice
Skin tissue
Spleen tissue
Serum sample
62.5 mg Vaseline or IMQ treatment in back skin
Day 0
Day 6
B
C
D
Spleen Index (mg/g)
E
F
Back skin thickness (mm)
Erythema PASI Score
Scales PASI Score
Days
G
H
Concentration level (pg/mL)
IL-27
IFN-γ
I
CD4+ IFN-γ+ T cells (%)
J
Skin
Spleen
IFN-γ-PE
CD4-FITC
K
PLCβ
p-PKC
PKC
p-p38
p38
p-JNK
JNK
β-actin
L
p-JAK2
JAK2
p-STAT1
STAT1
T-bet
M
Relative protein expression level
N
Relative mRNA expression
p28
Ebi3
Ifnγ
Cxcl9
Cxcl10
Cxcl11

DCs between WT and $P2Y_6R^{-/-}$ mice after IMQ treatment (Fig. S3G). In all, the above results indicated a correlation could exist between activated macrophage $P2Y_6R$ and Th1 cells involved in psoriasis processes.

3.2. *Macrophage $P2Y_6R$ mediates Th1 type psoriasis-like inflammation*

To further understand the mechanism of macrophage $P2Y_6R$ driven Th1 cell differentiation, we purified Naïve $CD4^+$ T-cells from WT mice and cultured these cells with culture supernatants collected from activated WT or $P2Y_6R^{-/-}$ BMDMs[12,13] (Fig. 2A). UDP, which was the natural ligand enriched in purine metabolism for $P2Y_6R$, was involved in the inflammation formation as previously reported[14-17]. Here, we used IMQ and UDP as the activator to stimulate macrophages. As expected, the supernatants from $P2Y_6R^{-/-}$ macrophages induced a lower percentage of IFN-γ^+ $CD4^+$ T-cells compared to the supernatants from WT macrophages (Fig. 2B and C). These findings were supported by the increasing mRNA expression levels of Th1 cytokines *Ifnγ*, *Cxcl9*, *Cxcl10, Cxcl11,* and the concentration of IFNγ in the supernatant was attenuated after $P2Y_6R^{-/-}$ macrophages supernatants intervention in $CD4^+$ T cell[18,19] (Fig. 2D and E). In addition, *P2ry6* was enriched among genes correlating positively with *Stat1* (Fig. 2F). According to GSEA and ChEA3 analysis, *Stat1* was identified as a highly ranked transcription factor and up-regulated *via* JAK/STAT signaling pathway in psoriasis (Fig. 2G and H). In $CD4^+$ T cells, stimulation with the supernatants from $P2Y_6R^{-/-}$ macrophages decreased the levels of p-JAK2, p-STAT1, and T-bet expression (Fig. 2I and J). Further, the reduction percentage of Th1 cells and mRNA level of *Ifnγ* induced by $P2Y_6R^{-/-}$ macrophages supernatants was greatly up-regulated after the JAK/STAT pathway agonist RO8191 intervention (Fig. 2K and L). Besides, pre-treatment with RO8191 showed the same effect in T-bet protein expression (Fig. 2M and N). Overall, our findings suggested that $P2Y_6R$ on macrophages regulated Th1 cell differentiation *via* p-JAK2/p-STAT1/T-bet signaling.

3.3. *Activated macrophages secrete IL-27 via $P2Y_6R$/PLC_β/p-PKC/MAPK axis*

To explore the signaling pathway responsible for psoriasis and assess how macrophage $P2Y_6R$ regulated Th1 cell differentiation, we selected the top 30 proteins in the PPI network based on their topological characteristics for further enrichment analysis (Fig. S2E). The top 15 KEGG pathways and GO biological process terms were shown (Fig. 3A, Supporting Information Fig. S5). The IL-27 signaling pathway was the most significantly enriched, while *P2ry6* expression was correlating positively with *Il27* (Fig. 3B). Based on these findings, it is necessary to clarify whether activated $P2Y_6R$ in macrophages triggered the release of IL-27. Thus, we measured IL-27 concentration in the supernatant of BMDMs from $P2Y_6R^{-/-}$ and WT mice, respectively (Fig. 3C). After UDP and IMQ intervention, the IL-27 concentration in $P2Y_6R^{-/-}$ BMDMs was significantly lower than WT BMDMs (Fig. 3D).

The previous study indicated that IL-27ra was predominantly expressed in $CD4^+$ T cells[20]. Next, to determine whether the $P2Y_6R$ stimulated macrophages-derived Th1 cell differentiation was driven by IL-27 dependently, we isolated Naïve $CD4^+$ T-cells from WT or IL-27ra$^{-/-}$ mice and cultured them with supernatants collected from activated WT or $P2Y_6R^{-/-}$ BMDMs, IL-27 recombinant protein was used as positive control (Fig. 3E). The supernatants of WT BMDMs significantly induced robust Th1 cell differentiation and IFNγ concentration in WT Naïve T cells compared to the supernatants from $P2Y_6R^{-/-}$ BMDMs. However, the supernatants of WT or $P2Y_6R^{-/-}$ macrophages showed no difference in enhancing Th1 differentiation and IFNγ secretion in the absence of IL27ra (Fig. 3F−H).

Next, we further investigated how activated $P2Y_6R$ in macrophages triggered the release of IL-27. It was reported that $P2Y_6R$ stimulation could activate PLC_β/p-PKC/MAPK downstream signaling and the Ca^{2+} influx[21-23]. In macrophages, p-JNK mediated the IL-27 release, and increased intracellular Ca^{2+} concentration is widely recognized to contribute to inflammatory macrophage activation[24-27] (Fig. 3I). The intracellular Ca^{2+} fluorescence intensity in $P2Y_6R^{-/-}$ BMDMs treated with IMQ and UDP was decreased compared to WT BMDMs (Fig. 3I and J). Furthermore, the expression levels of PLC_β, p-PKC, p-p38, and p-JNK were substantially decreased in IMQ and UDP-treated $P2Y_6R^{-/-}$ BMDMs, while p-ERK showed relatively lower expression, but the difference was not significant (Fig. 3K and L). As we thought, pre-treatment with PMA (PKC agonist), Anisomycin (JNK agonist), and Cigilitazone (p38 agonist), but not Ceramide C6 (ERK agonist), increased IL-27 concentration in $P2Y_6R^{-/-}$ BMDMs (Fig. 3M). These indicated that the mechanism by which activated $P2Y_6R$ triggered the release of IL-27 may relied on the activation of the PLC_β/p-PKC/MAPK axis in macrophages.

To verify the findings *in vitro*, an assay was performed in WT and $P2Y_6R^{-/-}$ mice *in vivo* (Supporting Information Fig. S6A). After IMQ-treated, the IL-27 and IFNγ concentrations in WT mice skin and serum were significantly increased, while attenuated in $P2Y_6R^{-/-}$ mice respectively (Fig. S6B). The up-regulation of several Th1 chemokines induced by IMQ was attenuated in $P2Y_6R^{-/-}$ mice (Fig. S6C). Besides, the protein expression levels of PLC_β, p-PKC, p-p38, p-JNK, p-JAK2, p-STAT1, and T-bet

Figure 4 IMQ-induced psoriasis mice is reduced in $Lyz2^{cre}P2Y_6R^{fl/fl}$ mice. (A) Experimental scheme. (B) Representative skin pictures of $Lyz2^{cre}P2Y_6R^{fl/fl}$ and $P2Y_6R^{fl/fl}$ mice. (C) Pictures of spleen and (D) spleen index from all groups ($n = 12$). (E, F) H&E staining ($n = 3$) and skin thickness, erythema, and scaling PASI score ($n = 12$) of IMQ or Vaseline-treated $Lyz2^{cre}$ $P2Y_6R^{fl/fl}$ and $P2Y_6R^{fl/fl}$ mice skin. (G) Ki67 staining of IMQ-treated skin tissues from $P2Y_6R^{fl/fl}$ or $Lyz2^{cre}P2Y_6R^{fl/fl}$ mice treated with Saline or IL-27 ($n = 3$). (H) Serum and skin concentrations of IL-27 and IFNγ detected by ELISA assay ($n = 4$). (I, J) Flow analysis of Th1 cells from skin and spleens of $Lyz2^{cre}P2Y_6R^{fl/fl}$ and $P2Y_6R^{fl/fl}$ mice treated with IMQ or Vaseline ($n = 3$). (K−M) Quantitative analysis of protein expression in mice skin. Normal protein levels were normalized to β-actin, and the values for the phosphorylated forms of proteins were normalized to phosphorylation-independent levels of the same protein. ($n = 4$). (N) The mRNA expression levels of Th1-related cytokine and IL-27 *p28* and *Ebi3* in skin tissues ($n = 3$). All mRNA levels were normalized to GAPDH mRNA. Data are expressed as mean ± SEM. $^*P < 0.05$, $^{**}P < 0.01$, $^{***}P < 0.001$.

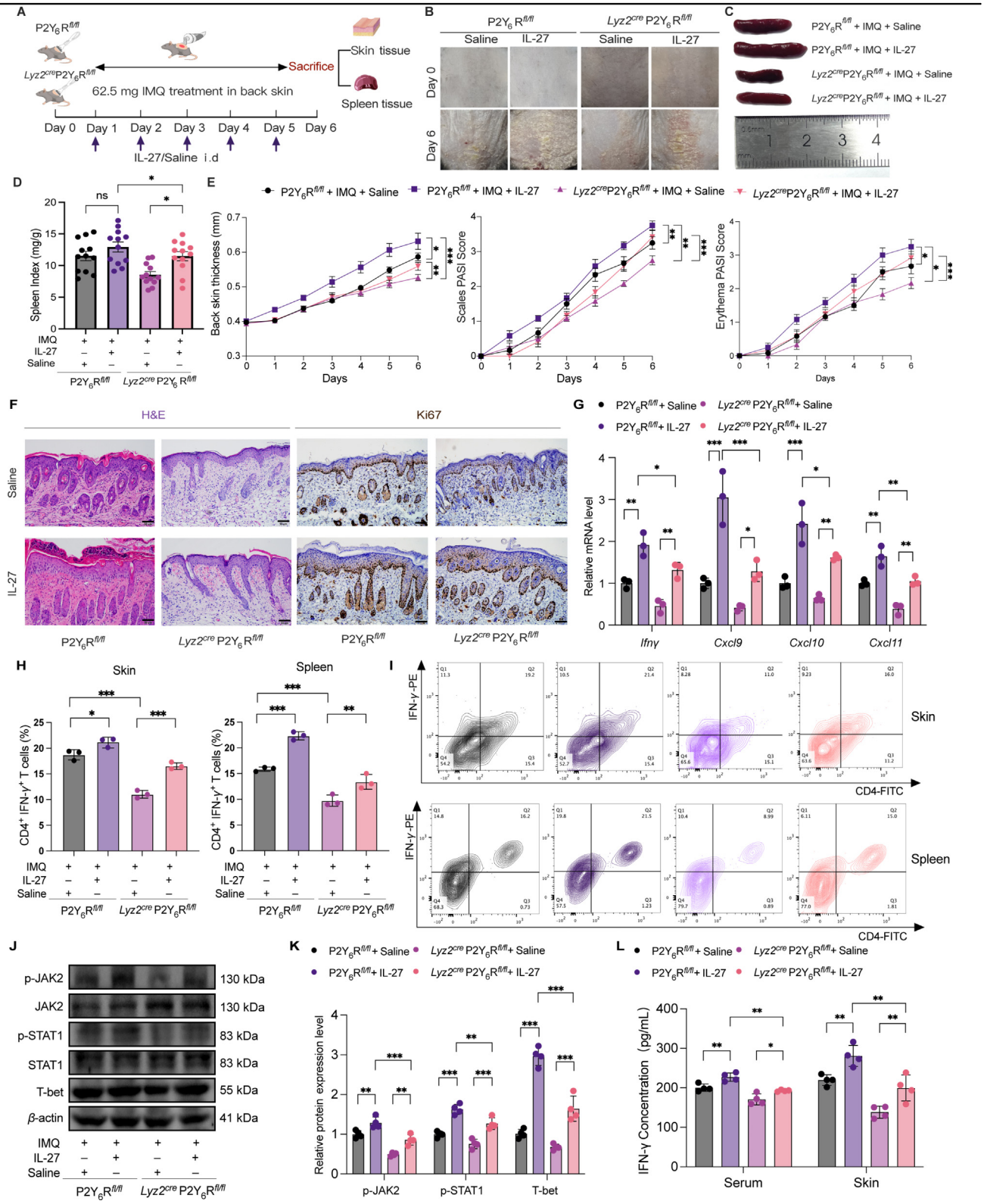

Figure 5 Increase of IL-27 restores psoriatic inflammation in *Lyz2*^{cre} P2Y$_6$R$^{fl/fl}$ mice. (A) Flow diagram. (B) Representative psoriatic plaque pictures of mice. (C) Pictures of the spleen. (D) Spleen index of all groups. (E, F) Skin thickness, erythema and scaling PASI score, H&E staining ($n = 3$), and Ki67 staining ($n = 3$) of IMQ-induced *Lyz2*^{cre}P2Y$_6$R$^{fl/fl}$ and P2Y$_6$R$^{fl/fl}$ mice skin treated with Saline or IL-27. (G) The mRNA expression levels of Th1-related cytokines in skin tissues from IMQ-induced mice treated with Saline or IL-27 ($n = 3$). All mRNA levels were normalized to GAPDH mRNA. (H, I) Flow analysis on Th1 cells from skin and spleens of all groups. IL-27 reversed the decrease of Th1 cells (CD4$^+$ IFNγ^+) proportion in IMQ-treated *Lyz2*^{cre}P2Y$_6$R$^{fl/fl}$ mice. (J, K) Quantitative analysis of protein expression in mice skin. Normal protein levels were normalized to β-actin, and the values for the phosphorylated forms of proteins were normalized to phosphorylation-independent levels of the same protein ($n = 4$). (L) Serum and skin concentrations of IL-27 and IFNγ detected by ELISA assay ($n = 4$). Data are expressed as mean ± SEM. $^*P < 0.05$, $^{**}P < 0.01$, $^{***}P < 0.001$.

were also decreased in IMQ-treated P2Y$_6$R$^{-/-}$ mice (Fig. S6D–S6G). Taken together, we concluded that the signaling cascade of P2Y$_6$R activation mediated the interaction between macrophages and T lymphocytes in psoriasis.

3.4. *IMQ-induced psoriasis is reduced in Lyz2^{cre}P2Y$_6$R$^{fl/fl}$ mice*

To further directly assess the cell type-intrinsic function of P2Y$_6$R in macrophages, we generated a conditional macrophage-specific P2Y$_6$R knockout mice (*Lyz2^{cre}*P2Y$_6$R$^{fl/fl}$). These mice with their P2Y$_6$R$^{fl/fl}$ littermates were treated with IMQ (Fig. 4A). As for the result, loss of P2Y$_6$R in macrophages alleviated IMQ-induced psoriatic inflammation and the proliferation of keratinocytes (Fig. 4B–G). ELISA result revealed that IL-27 and IFNγ level was significantly alleviated in *Lyz2^{cre}*P2Y$_6$R$^{fl/fl}$ mice treated with IMQ, but increased in IMQ-treated P2Y$_6$R$^{fl/fl}$ mice (Fig. 4H). The alleviation of disease severity was correlated with decreased number of Th1 cells in the skin and spleen (Fig. 4I and J). The protein expression of PLC$_\beta$, p-PKC, p-p38, p-JNK, p-JAK2, p-STAT1, and T-bet were decreased in IMQ-treated *Lyz2^{cre}*P2Y$_6$R$^{fl/fl}$ (Fig. 4K–M). Accordingly, the transcript levels of Th1-associated chemokines were also strongly down-regulated in *Lyz2^{cre}*P2Y$_6$R$^{fl/fl}$ mice treated with IMQ (Fig. 4N).

Considering the mRNA expression of *P2ry6* was relatively high in CD4$^+$ T cells (Fig. 1J), we further investigated the role of P2Y$_6$R in CD4$^+$ cells by using *CD4^{cre}*P2Y$_6$R$^{fl/fl}$ mice. After 5 days of IMQ treatment, there was no significant difference in the dermal thickness, PASI score, or spleen index observed between P2Y$_6$R$^{fl/fl}$ and CD4^{cre}P2Y$_6$R$^{fl/fl}$ mice (Supporting Information Fig. S7). Based on this, we inferred that the macrophage P2Y$_6$R was mainly responsible for increased severity of psoriasiform dermatitis, rather than P2Y$_6$R in CD4$^+$ T cells.

3.5. *IL-27 restores IMQ-induced psoriasis inflammatory phenotype in Lyz2^{cre}P2Y$_6$R$^{fl/fl}$ mice*

To confirm the mechanism by which P2Y$_6$R promoted IL-27-dependent production found in mouse macrophages. IL-27

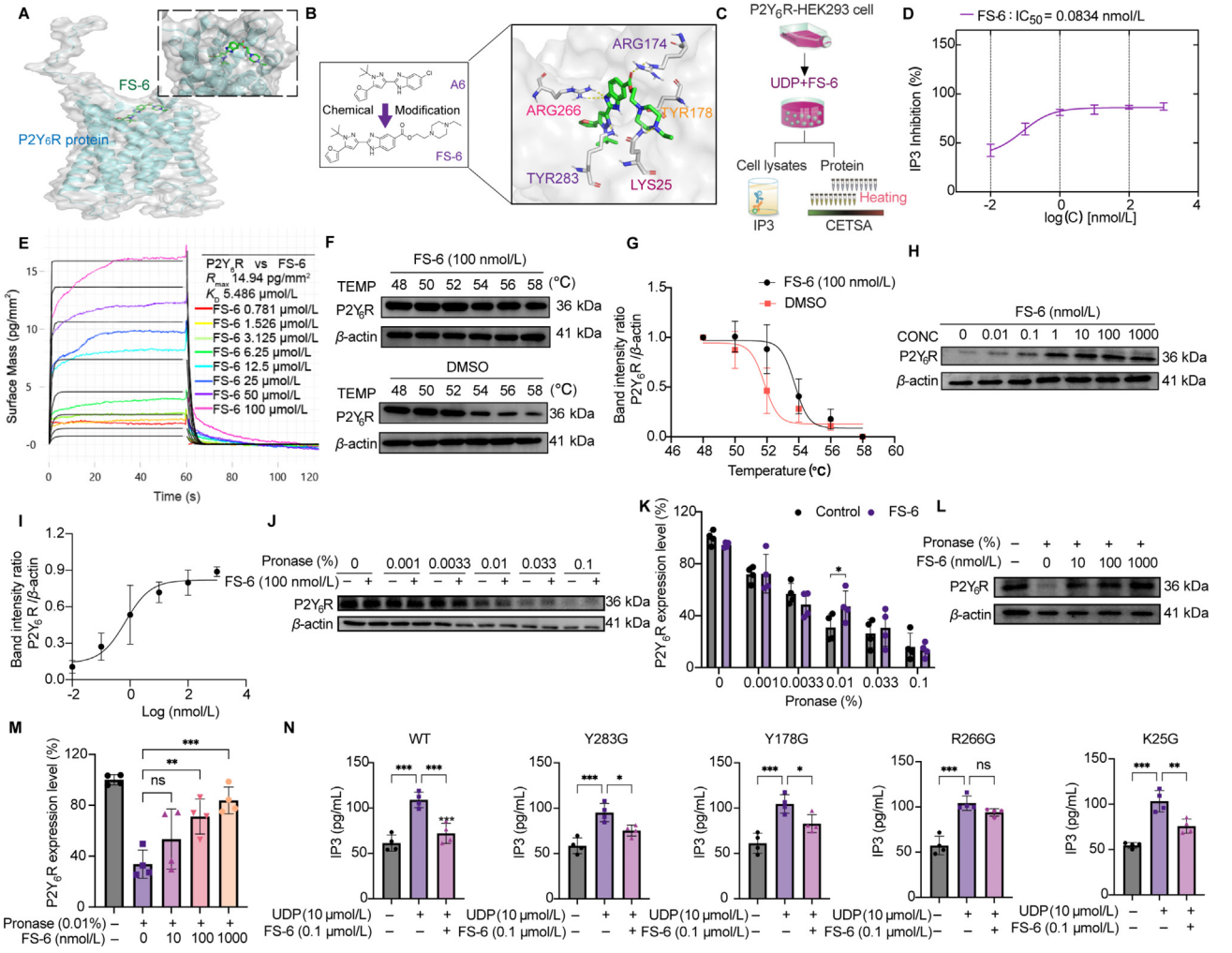

Figure 6 A novel P2Y$_6$R inhibitor FS-6 with excellent activity and binding affinity. (A) The overall structure of P2Y$_6$R with FS-6 bound. (B) Chemical modification from A6 to FS-6 and the possible binding sites between FS-6 and P2Y$_6$R. (C) Flow diagram of IC$_{50}$ value and binding activity of FS-6. (D) IC$_{50}$ curve of FS-6 was determined by ELISA ($n = 6$). (E) Direct binding between FS-6 and P2Y$_6$R. (F–I) The binding between FS-6 and P2Y$_6$R was evaluated by CETSA in P2Y$_6$R-HEK293 cells ($n = 4$). (J–M) The dose-dependent binding of FS-6 to P2Y$_6$R was evaluated by DARTs ($n = 4$). (N) Arg266Gly was verified as the binding site of FS-6 and P2Y$_6$R to detect IP3 concentration ($n = 4$). Data are expressed as mean ± SEM. *$P < 0.05$, **$P < 0.01$, ***$P < 0.001$. ns, not significant.

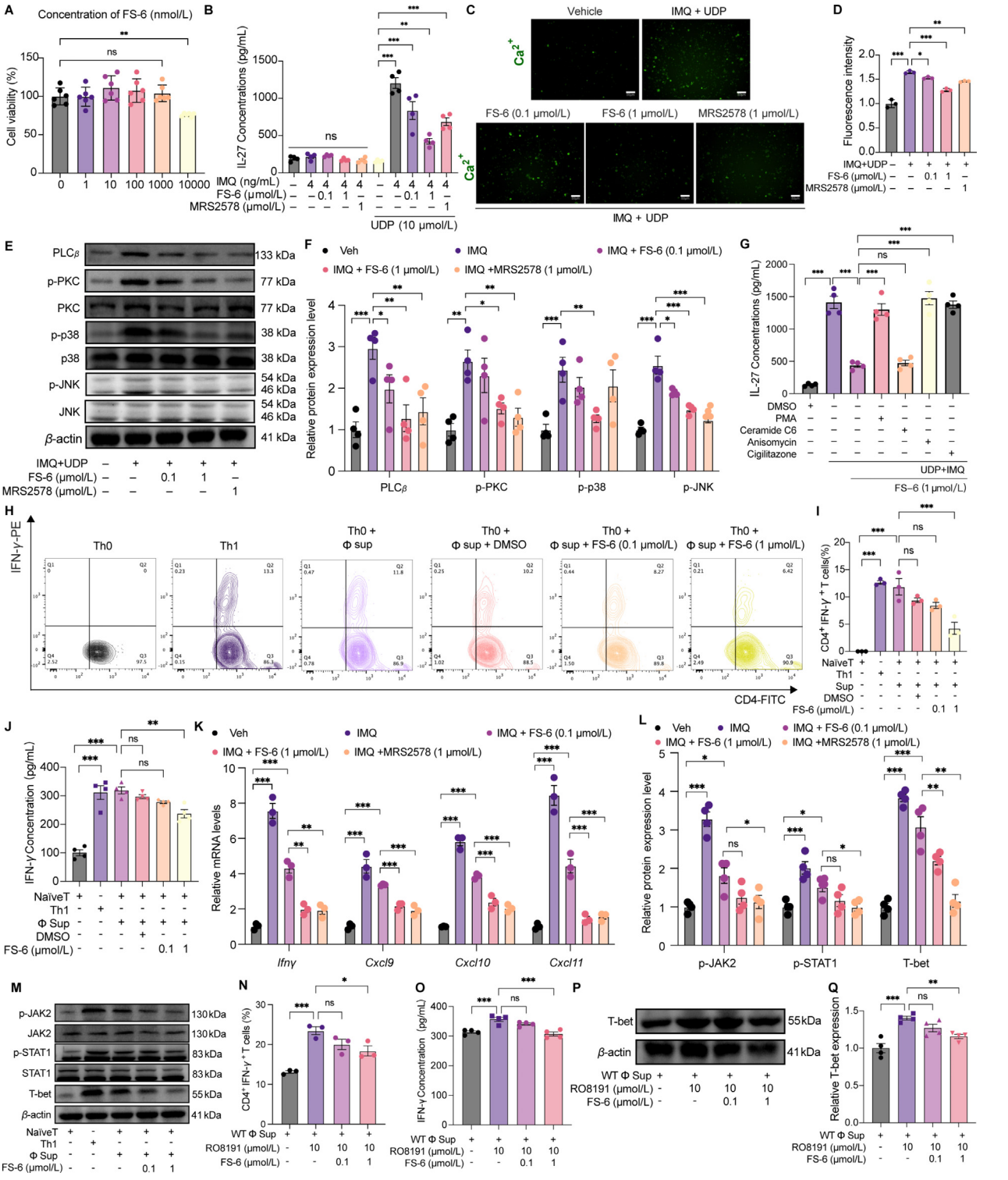

Figure 7 P2Y$_6$R inhibitor FS-6 regulates the secretion of IL-27 from macrophages thus inhibiting Th1 cell differentiation. (A) The effects of FS-6 on BMDMs viability ($n = 6$). (B) FS-6 decreased IL-27 concentration in BMDMs supernatant under the stimulation of UDP and IMQ ($n = 4$). (C, D) Changes in FS-6 treated BMDMs intracellular Ca^{2+} were measured and quantitative analysis of fluorescence intensity ($n = 3$).

recombinant protein was administered to *Lyz2*^{cre}P2Y$_6$R$^{fl/fl}$ and P2Y$_6$R$^{fl/fl}$ mice treated with IMQ, while saline was given as a control[28] (Fig. 5A). Consistent with the previous results, the skin inflammation was significantly decreased in IMQ-treated *Lyz2*^{cre}-P2Y$_6$R$^{fl/fl}$ mice compared to IMQ-treated P2Y$_6$R$^{fl/fl}$ mice. In contrast, IMQ-treated *Lyz2*^{cre}P2Y$_6$R$^{fl/fl}$ mice with IL-27 recombinant protein showed more severe psoriatic inflammation and keratinization compared to IMQ-treated *Lyz2*^{cre}P2Y$_6$R$^{fl/fl}$ mice treated with saline (Fig. 5B−F). Additionally, in *Lyz2*^{cre}P2Y$_6$R$^{fl/fl}$ mice, there was an increase in the proportion of IFNγ^+ CD4$^+$ Th1-cells in the skin and spleen after IL-27 administration (Fig. 5G−I). The decreased mRNA expression levels of *Ifnγ*, *Cxcl9*, *Cxcl10,* and *Cxcl11* and the protein expression levels of JAK2, STAT1, T-bet were significantly restored in IMQ-induced *Lyz2*^{cre}P2Y$_6$R$^{fl/fl}$ mice by intradermal IL-27 injection (Fig. 5J−L). In all, these results provided compelling evidence that the elevation of IL-27 restores the reduced psoriatic inflammation caused by macrophage P2Y$_6$R deficiency.

3.6. *The discovery of a novel P2Y$_6$R inhibitor FS-6*

We next tried to find a P2Y$_6$R inhibitor with excellent inhibitory activity and binding affinity to further verify the role of P2Y$_6$R in psoriasis. In our previous study, a potent P2Y$_6$R inhibitor A6 with a novel scaffold was discovered[29,34]. However, A6 had limitations in terms of poor aqueous solubility and bio-availability, hindering its further development. To address this, we performed docking of A6 with the homology model of P2Y$_6$R. We discovered that the furan ring of A6 is deeply buried in the hydrophobic pocket, while the substituent on the benzimidazole end is exposed in the solvent (Fig. 6A). Therefore, to improve the aqueous solubility of the compound while retaining its antagonistic activity, we rationally designed and synthesized a series of polar groups substituted on the benzimidazole substituent with different linkers (Fig. 6B). The optimized compound FS-6 (P2Y$_6$R IC$_{50}$ = 0.0834 nmol/L)[34] showed strong binding ability to P2Y$_6$R, and notably improved solubility (5.029 mg/mL in water) (Fig. 6C and D, Supporting Information Table S4, Scheme S1). The GCI results revealed a dose-dependent interaction between FS-6 and P2Y$_6$R (Fig. 6E). In the CETSA assay, the maximum difference in the stability of FS-6 and P2Y$_6$R is observed at 54 °C, and the stabilization effect of FS-6 on P2Y$_6$R showed dose-dependency (Fig. 6F−I). The DARTs assay showed the increased stability of P2Y$_6$R against pronase after treating FS-6 (Fig. 6J and K). Notably, the stability of P2Y$_6$R was increased in a dose-dependent manner by FS-6 (Fig. 6L and M). To further investigate the key residues involved in the binding of FS-6 to P2Y$_6$R, we compared the docking modes of A6, FS-6, and MRS2578 with P2Y$_6$R. We discovered that both A6 and FS-6 bind to the same pocket, whereas MRS2578 binds at a different site due to its role as a covalent inhibitor of P2Y$_6$R (Supporting Information Fig. S8A and S8B). Besides the nitrogen atoms on the benzimidazole rings of A6 and FS-6 form stable hydrogen bond interactions with the ARG266 residue (Fig. S8C). Based on the result of the docking simulation, we generated point mutation at each of these residues (Y283G, R266G, Y178G, K25G) in P2Y$_6$R-HEK293 cells (Supporting Information Fig. S9). The mutation of ARG266 on P2Y$_6$R resulted in a complete loss of inhibitory activity of FS-6 (Fig. 6N). In conclusion, we discovered a novel P2Y$_6$R inhibitor, FS-6, which exhibits potent inhibitory activity and excellent water solubility, making it a promising candidate for further research and development.

3.7. *FS-6 attenuates Th1 cell differentiation which ameliorates IMQ-induced psoriasis*

Given FS-6 has such excellent activity and binding affinity of P2Y$_6$R, we assessed its ability to suppress macrophage IL-27 production. The well-recognized P2Y$_6$R inhibitor MRS2578 was used as a positive control[35-37]. CCK-8 assay was used to determine the optimal drug concentration of FS-6 (Fig. 7A). After co-stimulation with IMQ and UDP, treatment with FS-6 resulted in a dose-dependent decrease in IL-27 and intracellular Ca^{2+} concentration significantly (Fig. 7B−D). The administration of FS-6 led to a decreased PLC$_\beta$, p-PKC, p-p38, and p-JNK protein expression (Fig. 7E and F). While related agonists could reverse the IL-27 response in the FS-6 treatment group (Fig. 7G). The macrophage supernatant containing FS-6 effectively reduced Th1 cell differentiation and IFNγ concentration (Fig. 7H−J), accompanied by the down-regulation of T cell chemokines mRNA expression (Fig. 7K). Furthermore, the expression protein levels in Naïve T cells were also significantly decreased after FS-6 intervention (Fig. 7L and M). Additionally, RO8191 markedly reversed the decreased proportion of Th1 cells, the secretion of IFNγ, and the expression of T-bet protein was induced by FS-6 treatment (Fig. 7N−P).

To evaluate the effect of FS-6 *in vivo*, WT mice applied with IMQ and received daily doses of FS-6 (10 and 20 mg/kg, i.p). Methotrexate (MTX) (1 mg/kg, i.p) served as the positive control[38] (Fig. 8A). After 5 days of treatment, mice treated with

(E, F) FS-6 decreased protein expression in BMDMs stimulated by UDP and IMQ. Normal protein levels were normalized to β-actin, and the values for the phosphorylated forms of proteins were normalized to phosphorylation-independent levels of the same protein (n = 4). (G) IL-27 supernatant concentration of BMDMs stimulated by UDP and IMQ after PKC, JNK, p38, and ERK agonist treatment. (H, I) The proportion of Th1 cells induced by WT BMDMs supernatant was decreased under the treatment of FS-6 (n = 3). (J) FS-6 decreased CD4$^+$ Naïve T-cells supernatant IFNγ concentration after BMDMs supernatant inducing (n = 4). (K) FS-6 decreased the mRNA expression levels of the Th1-associated cytokines, *Ifnγ*, *Cxcl9*, *Cxcl10* and *Cxcl11* (n = 3). (L, M) FS-6 decreased protein expression in T cells (n = 4). (N) The proportion of Th1 cells induced by WT BMDMs supernatant and JAK/STAT agonist was decreased under the treatment of FS-6 (n = 3). (O) FS-6 decreased supernatant IFNγ concentration of Th1 cells induced by WT BMDMs supernatant and JAK/STAT agonist (n = 4). (P, Q) FS-6 decreased the T-bet expression level of Th1 cells induced by WT BMDMs supernatant and JAK/STAT agonist (n = 4). Data are expressed as mean ± SEM. *P < 0.05, **P < 0.01, ***P < 0.001.

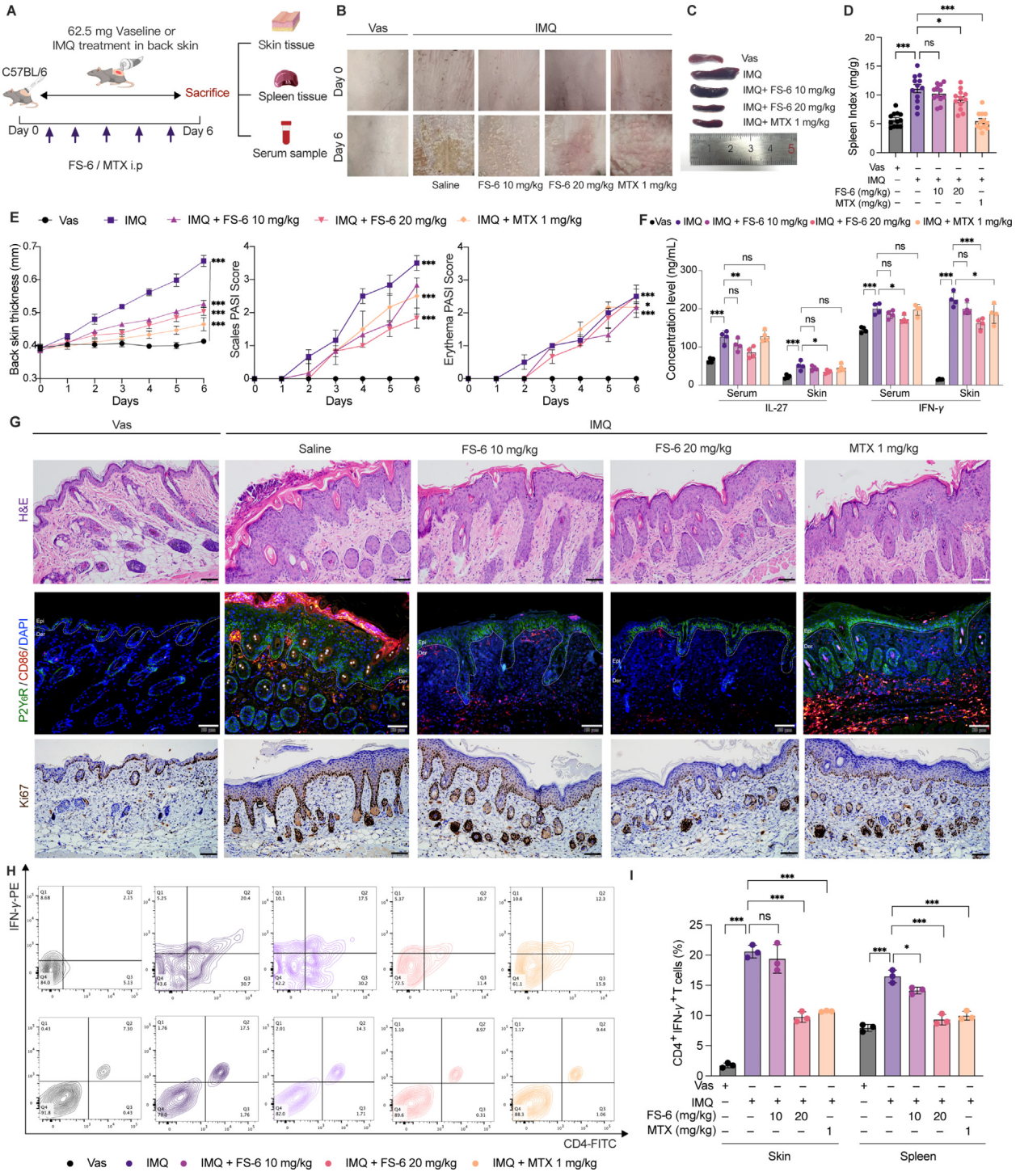

Figure 8 FS-6 ameliorates IMQ-induced psoriasis in mice. (A) Experimental scheme for assessment of psoriasiform dermatitis ($n = 12$). (B) Representative skin pictures. (C) Picture of spleen and (D) spleen index from all groups ($n = 12$). (E) PASI score ($n = 12$). (F) Serum and skin concentrations of IL-27 and IFNγ ($n = 4$). (G) FS-6 reduced epidermal thickening, keratinocyte proliferation, and co-localization of macrophages and $P2Y_6R$ ($n = 3$). (H, I) Flow analysis on Th1 cells from skin and spleens of mice ($n = 3$). Data are expressed as mean ± SEM. $^*P < 0.05$, $^{**}P < 0.01$, $^{***}P < 0.001$.

FS-6 showed a significant reduction in epidermal thickness and dermal inflammation compared to the model group (Fig. 8B–E). Moreover, the IL-27 and IFNγ content was decreased after administration of FS-6 in the mice serum and skin (Fig. 8F). Additionally, H&E and Ki67 staining of the skin confirmed the therapeutic effect of FS-6 in psoriasis mice, and FS-6 administration could reduce $P2Y_6R^+$ $CD86^+$ double-positive macrophages in mice dermis (Fig. 8G).

We then explored whether administration of FS-6 could suppress the differentiation of Th1 cells. Compared to the model

group, the Th1 cell differentiation rate in mice spleen and skin lesions was significantly decreased after FS-6 was administered (Fig. 8H and I). Given the role of $P2Y_6R$ *in vitro*, we next confirmed whether FS-6 inhibits $P2Y_6R$-meditated downstream signaling pathway *in vivo* (Supporting Information Fig. S10A and S10B). Notably, FS-6 significantly inhibited the mRNA expression levels of *Ifnγ*, *Cxcl9*, *Cxcl10*, *Cxcl11* and two submits of IL-27, *p28* and *Ebi3* (Fig. S10C). Collectively, these data confirmed that targeted $P2Y_6R$ was a potential therapeutic strategy in psoriasis.

4. Discussion

$P2Y_6R$ has been implicated in the pathogenesis of inflammatory bowel disease, atherosclerosis, Parkinson's disease, and remodeling in experimental allergic airway inflammation[14,16,17,34-36,39-41]. Due to its pro-inflammatory activity, $P2Y_6R$ is highly abundant in a wide range of immune cells, including macrophages and T cells. M1 macrophages significantly promote dermatitis pathogenesis in a psoriasis-like mouse model[42]. Besides, treatments that target M1 macrophage activation may serve as a general therapeutic candidate for psoriasis[43,44]. Here, we demonstrated that $P2Y_6R$ was up-regulated in psoriasis and was co-localized with $CD86^+$ M1 macrophages. The deficiency of $P2Y_6R$ hindered the progression of psoriasis.

Extracellular UDP, released as a danger signal by stressed or apoptotic cells, played an important role in a series of physiological processes[45]. In innate immune responses, macrophages release UDP as damage-associated molecular pattern molecules cause inflammation[46,47]. Besides, our previous studies have shown that macrophage $P2Y_6R$ was activated by UDP and played a role in immune response and inflammation modulation[22]. In the present study, we found that UDP, along with IMQ, mediated the activation of macrophagic $P2Y_6R$, leading to the activation of PLC_β/p-PKC/MAPK signaling pathways, which ultimately triggered the release of IL-27. In the MAPK pathway, JNK signaling is a commonly dysregulated signaling pathway in various human diseases, including psoriasis[48]. JNK activation is known to be mediated by IP3 Ca^{2+} stores, while $P2Y_6R$ couples to Gq protein, activating PLC_β, resulting in increased intracellular Ca^{2+} level[22,49,50]. Additionally, $P2Y_6R$-mediated JNK activation in metabolic dysfunction has been reported previously[41]. Therefore, we hypothesized that the activation of the UDP positive feedback loop may result in the persistent activation of macrophagic $P2Y_6R$ in psoriasis, contributing to its pathogenesis.

IL-27 level was observed to be higher in both the serum and the diseased tissue in psoriatic patients, and this increase correlated with the severity of the disease[51]. Moreover, IL-27 injected locally aggravated the progression in the IMQ-induced mouse psoriasis model[28]. Therefore, inhibition of IL-27 was considered a potential strategy for preventing of psoriasis[52]. Mechanically, IL-27 is primarily produced by activated antigen-presenting cells and plays an important role in the regulation of $CD4^+$ Th1 cell differentiation and immune response[53-56]. We observed the same phenomenon in macrophages stimulated with IMQ and UDP, while IL-27 production was significantly decreased following $P2Y_6R$ depletion. In accordance with the GO enrichment and GSEA analysis results, $P2Y_6R$ induced the relevant interaction between macrophages and Th1 cells, and this interaction was mediated by IL-27.

Previous literature reported that $P2Y_6R$ can promote the differentiation of Th1 cells in intestinal inflammation[39]. Th1 cells produce *Ifnγ* and T-bet and play a pathogenic role in psoriasis[57]. It has been reported that IL-27 induces STAT-1 phosphorylation and increases T-bet expression[58]. The dysregulated p-JAK2-p-STAT1 signaling axis in psoriasis has been implicated in the increased expression of cytokines, such as IFN-γ, which contributed to the pro-inflammatory environment in psoriatic lesions[59-61]. Collectively, our data showed that $P2Y_6R$ had critical functions in macrophages, including the promotion of pro-inflammatory cytokine IL-27, while IL-27 induced Th1 cell differentiation *via* p-JAK2/p-STAT1/T-bet axis, ultimately exacerbating the psoriasis progression.

Developing small-molecule inhibitors targeting $P2Y_6R$ has been challenging due to the lack of a resolved crystal structure and the absence of key residues on the binding sites. In our previous study, a potent $P2Y_6R$ inhibitor A6 with a novel scaffold was discovered[29,34]. However, the poor aqueous solubility and bioavailability of A6 have hindered further pharmacological research and development. The chemical optimization on the benzimidazole ring of A6 may be a promising strategy for $P2Y_6R$ inhibitors with improved aqueous solubility and bioavailability. In this study, we utilized docking modes and binding free energy calculations from prior research to design mutagenesis experiments on the $P2Y_6R$, ARG266, which demonstrated a complete loss of inhibitory activity by FS-6, indicating a promising small-molecule binding site. Besides, the FS-6 therapeutic mechanism may avoid the currently observed lack of selectivity in psoriasis small molecule therapeutics such as JAK inhibitors and the prevalent gastrointestinal adverse effects associated with PDE4 inhibitors[3]. Additionally, monoclonal antibodies, which are commonly employed in the treatment of psoriasis, are expensive and require administration *via* injection[1]. FS-6 offers a more accessible oral dosing option. This potential for oral delivery not only enhances patient convenience but also promises a more cost-effective solution. In conclusion, FS-6 may serve as a framework to guide the discovery of inhibitors for $P2Y_6R$.

However, our study contains several limitations. Although the mechanism underlying cross-talk between IL-27RA in Th1 cells and $P2Y_6R$ in macrophages has been uncovered. However, a more complex mechanism, involving the resolution of $P2Y_6R$ crystal structure would be required. Targeted drugs for macrophage $P2Y_6R$ in treating psoriasis remain to be developed and explored. In summary, our present study provided evidence of mechanism underlying $P2Y_6R$ in the pathogenesis of psoriasis and highlighted the potential of $P2Y_6R$ inhibitors as drug candidates for psoriasis therapy. On the other hand, FS-6 displayed inhibitory effects on psoriasis progression as a novel $P2Y_6R$ inhibitor, which confirmed the feasibility of $P2Y_6R$ targeted therapy on psoriasis.

Acknowledgments

This work was supported by the funds from National Natural Science Foundation of China (No. 82304506, No. 82373887, No. 82373725), the China Postdoctoral Science Foundation (2022M723513, China). We thank Dr. Qian Wang (Jinan University, Guangzhou, China) for the generous gift of the $IL\text{-}27ra^{-/-}$ mice line and we acknowledge Prof. Xinming Jia and Dr. Yao Yu

(Shanghai Tenth People's Hospital, School of Medicine, Tongji University, Shanghai, China) for sharing *CD4*^{cre} mice line.

Author contributions

Li Yin: Data curation, Formal analysis, Investigation, Methodology, Validation, Writing − original draft, Writing − review & editing. Enming Zhang: Data curation, Formal analysis, Software, Supervision, Validation, Visualization. Tianqi Mao: Data curation, Methodology, Resources, Validation, Visualization. Yifan Zhu: Data curation, Formal analysis, Methodology. Shurui Ni: Data curation, Methodology, Resources. Yehong Li: Writing − review & editing. Chunxiao Liu: Writing − review & editing. Yafei Fang: Writing − review & editing. Kexin Ni: Data curation, Formal analysis. Yuhe Lu: Data curation, Methodology. Huanqiu Li: Conceptualization, Data curation, Funding acquisition, Project administration, Supervision, Validation, Visualization, Writing − original draft, Writing − review & editing. Mengze Zhou: Conceptualization, Data curation, Funding acquisition, Project administration, Resources, Supervision, Validation, Visualization, Writing − original draft, Writing − review & editing. Qinghua Hu: Conceptualization, Data curation, Funding acquisition, Resources, Supervision, Validation, Visualization, Writing − original draft, Writing − review & editing.

Conflicts of interest

The authors declare that they have no competing interests.

Appendix A. Supporting information

Supporting information to this article can be found online at https://doi.org/10.1016/j.apsb.2024.06.008.

References

1. Griffiths CEM, Armstrong AW, Gudjonsson JE, Barker JNWN. Psoriasis. *Lancet* 2021;**397**:1301−15.
2. Uppala R, Tsoi LC, Harms PW, Wang B, Billi AC, Maverakis E, et al. "Autoinflammatory psoriasis"-genetics and biology of pustular psoriasis. *Cell Mol Immunol* 2021;**18**:307−17.
3. Bieber T. Disease modification in inflammatory skin disorders: opportunities and challenges. *Nat Rev Drug Discov* 2023;**22**:662−80.
4. Antonioli L, Blandizzi C, Pacher P, Haskó G. The purinergic system as a pharmacological target for the treatment of immune-mediated inflammatory diseases. *Pharmacol Rev* 2019;**71**:345−82.
5. Ferrari D, Casciano F, Secchiero P, Reali E. Purinergic signaling and inflammasome activation in psoriasis pathogenesis. *Int J Mol Sci* 2021;**22**:9449.
6. Cronstein BN, Sitkovsky M. Adenosine and adenosine receptors in the pathogenesis and treatment of rheumatic diseases. *Nat Rev Rheumatol* 2017;**13**:41−51.
7. Burnstock G, Knight GE, Greig AVH. Purinergic signaling in healthy and diseased skin. *J Invest Dermatol* 2012;**132**:526−46.
8. Di Virgilio F, Sarti AC, Coutinho-Silva R. Purinergic signaling, DAMPs, and inflammation. *Am J Physiol Cel Physiol* 2020;**318**:C832−5.
9. Di Virgilio F, Schmalzing G, Markwardt F. The elusive P2X7 macropore. *Trends Cel Biol* 2018;**28**:392−404.
10. Wagner EF, Schonthaler HB, Guinea-Viniegra J, Tschachler E. Psoriasis: what we have learned from mouse models. *Nat Rev Rheumatol* 2010;**6**:704−14.
11. Zhu Y, Wu Z, Yan W, Shao F, Ke B, Jiang X, et al. Allosteric inhibition of SHP2 uncovers aberrant TLR7 trafficking in aggravating psoriasis. *EMBO Mol Med* 2022;**14**:e14455.
12. Yong L, Yu Y, Li B, Ge H, Zhen Q, Mao Y, et al. Calcium/calmodulin-dependent protein kinase IV promotes imiquimod-induced psoriatic inflammation *via* macrophages and keratinocytes in mice. *Nat Commun* 2022;**13**:4255.
13. Zhao T, Wang Z, Fang J, Cheng W, Zhang Y, Huang J, et al. HTLV-1 activates YAP *via* NF-κB/p65 to promote oncogenesis. *Proc Natl Acad Sci U S A* 2022;**119**:e2115316119.
14. Koizumi S, Shigemoto-Mogami Y, Nasu-Tada K, Shinozaki Y, Ohsawa K, Tsuda M, et al. UDP acting at P2Y6 receptors is a mediator of microglial phagocytosis. *Nature* 2007;**446**:1091−5.
15. Steculorum SM, Paeger L, Bremser S, Evers N, Hinze Y, Idzko M, et al. Hypothalamic UDP increases in obesity and promotes feeding *via* P2Y6-dependent activation of AgRP neurons. *Cell* 2015;**162**:1404−17.
16. Qin J, Zhang Z, Fu Z, Ren H, Liu M, Qian M, et al. The UDP/P2y6 axis promotes lung metastasis of melanoma by remodeling the pre-metastatic niche. *Cel Mol Immunol* 2020;**17**:1269−71.
17. Umpierre AD, Li B, Ayasoufi K, Simon WL, Zhao S, Xie M, et al. Microglial P2Y6 calcium signaling promotes phagocytosis and shapes neuroimmune responses in epileptogenesis. *Neuron* 2024;**10**:S0896-6273(24)00195-8.
18. Renert-Yuval Y, Del Duca E, Pavel AB, Fang M, Lefferdink R, Wu J, et al. The molecular features of normal and atopic dermatitis skin in infants, children, adolescents, and adults. *J Allergy Clin Immunol* 2021;**148**:148−63.
19. Goldberg MF, Roeske EK, Ward LN, Pengo T, Dileepan T, Kotov DI, et al. Salmonella persist in activated macrophages in T cell-sparse granulomas but are contained by surrounding CXCR3 ligand-positioned Th1 Cells. *Immunity* 2018;**49**:1090−102.
20. Lu D, Lu J, Ji X, Ji Y, Zhang Z, Peng H, et al. IL-27 suppresses airway inflammation, hyperresponsiveness and remodeling *via* the STAT1 and STAT3 pathways in mice with allergic asthma. *Int J Mol Med* 2020;**46**:641−52.
21. Hennigs JK, Lüneburg N, Stage A, Schmitz M, Körbelin J, Harbaum L, et al. The P2-receptor-mediated Ca^{2+} signalosome of the human pulmonary endothelium−implications for pulmonary arterial hypertension. *Purinergic Signal* 2019;**15**:299−311.
22. Li Y, Zhou M, Li H, Dai C, Yin L, Liu C, et al. Macrophage P2Y6 receptor deletion attenuates atherosclerosis by limiting foam cell formation through phospholipase Cβ/store-operated calcium entry/calreticulin/scavenger receptor A pathways. *Eur Heart J* 2023;**00**:1−16.
23. Ma Y, Ran D, Zhao H, Shi X, Song R, Zou H, et al. The effect of P2X7R- mediated Ca^{2+} and MAPK signaling in OPG-induced duck embryo osteoclasts differentiation and adhesive structure damage. *Life Sci* 2022;**293**:120337.
24. Roewe J, Higer M, Riehl DR, Gericke A, Radsak MP, Bosmann M. Neuroendocrine modulation of IL-27 in macrophages. *J Immunol* 2017;**199**:2503−14.
25. Lou F, Sun Y, Xu Z, Niu L, Wang Z, Deng S, et al. Excessive polyamine generation in keratinocytes promotes self-RNA sensing by dendritic cells in Psoriasis. *Immunity* 2020;**53**:204−16.
26. Dominguez-Villar M, Gautron A-S, de Marcken M, Keller MJ, Hafler DA. TLR7 induces anergy in human $CD4^+$ T cells. *Nat Immunol* 2015;**16**:118−28.
27. Atcha H, Jairaman A, Holt JR, Meli VS, Nagalla RR, Veerasubramanian PK, et al. Mechanically activated ion channel Piezo1 modulates macrophage polarization and stiffness sensing. *Nat Commun* 2021;**31**:3256.
28. Shibata S, Tada Y, Asano Y, Yanaba K, Sugaya M, Kadono T, et al. IL-27 activates Th1-mediated responses in imiquimod-induced psoriasis-like skin lesions. *J Invest Dermatol* 2013;**133**:479−88.
29. Zhu Y, Zhou M, Cheng X, Wang H, Li Y, Guo Y, et al. Discovery of selective P2Y6R antagonists with high affinity and *in vivo* efficacy for inflammatory disease therapy. *J Med Chem* 2023;**66**:6315−32.

30. Zhang Z, Fan F, Luo W, Zhao Y, Wang C. Molecular Dynamics Revealing a detour-forward release mechanism of tacrine: implication for the specific binding characteristics in butyrylcholinesterase. *Front Chem* 2020;**8**:730.
31. Onufriev A, Bashford D, Case DA. Exploring protein native states and large-scale conformational changes with a modified generalized born model. *Proteins* 2004;**55**:383−94.
32. Weiser J, Shenkin PS, Still WC. Approximate atomic surfaces from linear combinations of pairwise overlaps (LCPO). *J Comput Chem* 1999;**20**:217−30.
33. Gohlke H, Kiel C, Case DA. Insights into protein-protein binding by binding free energy calculation and free energy decomposition for the Ras-Raf and Ras-RalGDS complexes. *J Mol Biol* 2003;**330**:891−913.
34. Tian S, Wang J, Li Y, Li D, Xu L, Hou T. The application of *in silico* drug-likeness predictions in pharmaceutical research. *Adv Drug Deliv Rev* 2015;**86**:2−10.
35. Salem M, Lecka J, Pelletier J, Gomes Marconato D, Dumas A, Vallières L, et al. NTPDase8 protects mice from intestinal inflammation by limiting P2Y6 receptor activation: identification of a new pathway of inflammation for the potential treatment of IBD. *Gut* 2022;**71**:43−54.
36. Vieira RP, Müller T, Grimm M, von Gernler V, Vetter B, Dürk T, et al. Purinergic receptor type 6 contributes to airway inflammation and remodeling in experimental allergic airway inflammation. *Am J Respir Crit Care Med* 2011;**184**:215−23.
37. Nishimura A, Sunggip C, Oda S, Numaga-Tomita T, Tsuda M, Nishida M. Purinergic P2Y receptors: molecular diversity and implications for treatment of cardiovascular diseases. *Pharmacol Ther* 2017;**180**:113−28.
38. Bharadwaj R, Lusi CF, Mashayekh S, Nagar A, Subbarao M, Kane GI, et al. Methotrexate suppresses psoriatic skin inflammation by inhibiting muropeptide transporter SLC46A2 activity. *Immunity* 2023;**56**:998−1012.
39. Nishiyama K, Nishimura A, Shimoda K, Tanaka T, Kato Y, Shibata T, et al. Redox-dependent internalization of the purinergic P2Y6 receptor limits colitis progression. *Sci Signal* 2022;**15**:eabj0644.
40. Yang X, Lou Y, Liu G, Wang X, Qian Y, Ding J, et al. Microglia P2Y6 receptor is related to Parkinson's disease through neuroinflammatory process. *J Neuroinflammation* 2017;**14**:38.
41. Salem M, El Azreq M-A, Pelletier J, Robaye B, Aoudjit F, Sévigny J. Exacerbated intestinal inflammation in P2Y6 deficient mice is associated with Th17 activation. *Biochim Biophys Acta, Mol Basis Dis* 2019;**1865**:2595−605.
42. Hou Y, Zhu L, Tian H, Sun HX, Wang R, Zhang L, et al. IL-23-induced macrophage polarization and its pathological roles in mice with imiquimod-induced psoriasis. *Protein Cell* 2018;**9**:1027−38.
43. Yang L, Fu J, Han X, Zhang C, Xia L, Zhu R, et al. Hsa_circ_0004287 inhibits macrophage-mediated inflammation in an *N*6-methyladenosine-dependent manner in atopic dermatitis and psoriasis. *J Allergy Clin Immunol* 2022;**149**:2021−33.
44. Sun Q, Hu S, Lou Z, Gao J. The macrophage polarization in inflammatory dermatosis and its potential drug candidates. *Biomed Pharmacother* 2023;**161**:114469.
45. Jain S, Pydi SP, Toti KS, Robaye B, Idzko M, Gavrilova O, et al. Lack of adipocyte purinergic P2Y6 receptor greatly improves whole body glucose homeostasis. *Proc Natl Acad Sci U S A* 2020;**117**:30763−74.
46. Qin J, Zhang G, Zhang X, Tan B, Lv Z, Liu M, et al. TLR-activated gap junction channels protect mice against bacterial infection through extracellular UDP release. *J Immunol* 2016;**196**:1790−8.
47. Obba S, Hizir Z, Boyer L, Selimoglu-Buet D, Pfeifer A, Michel G, et al. The PRKAA1/AMPKα1 pathway triggers autophagy during CSF1-induced human monocyte differentiation and is a potential target in CMML. *Autophagy* 2015;**11**:1114−29.
48. Hammouda MB, Ford AE, Liu Y, Zhang JY. The JNK signaling pathway in inflammatory skin disorders and cancer. *Cells* 2020;**9**:857.
49. Balogh J, Wihlborg AK, Isackson H, Joshi BV, Jacobson KA, Arner A, et al. Phospholipase C and cAMP-dependent positive inotropic effects of ATP in mouse cardiomyocytes *via* P2Y11-like receptors. *J Mol Cel Cardiol* 2005;**39**:223−30.
50. Enslen H, Tokumitsu H, Stork PJ, Davis RJ, Soderling TR. Regulation of mitogen-activated protein kinases by a calcium/calmodulin-dependent protein kinase cascade. *Proc Natl Acad Sci U S A* 1996;**93**:10803−8.
51. Tojo G-I, Fujimura T, Kambayashi Y, Aiba S. Systemic lupus erythematosus accompanied by psoriasis induces IL-27-producing cells in both affected areas of the skin. *Case Rep Dermatol* 2012;**4**:181−5.
52. Shibata S, Tada Y, Kanda N, Nashiro K, Kamata M, Karakawa M, et al. Possible roles of IL-27 in the pathogenesis of psoriasis. *J Invest Dermatol* 2010;**130**:1034−9.
53. Meka RR, Venkatesha SH, Dudics S, Acharya B, Moudgil KD. IL-27-induced modulation of autoimmunity and its therapeutic potential. *Autoimmun Rev* 2015;**14**:1131−41.
54. Lowes MA, Suárez-Fariñas M, Krueger JG. Immunology of psoriasis. *Annu Rev Immunol* 2014;**32**:227−55.
55. Wang Q, Ning H, Peng H, Wei L, Hou R, Hoft DF, et al. Tristetraprolin inhibits macrophage IL-27-induced activation of antitumour cytotoxic T cell responses. *Nat Commun* 2017;**8**:867.
56. Wong CK, Chen DP, Tam LS, Li EK, Yin YB, Lam CWK. Effects of inflammatory cytokine IL-27 on the activation of fibroblast-like synoviocytes in rheumatoid arthritis. *Arthritis Res Ther* 2010;**12**:R129.
57. Seder RA, Gazzinelli R, Sher A, Paul WE. Interleukin 12 acts directly on CD4+ T cells to enhance priming for interferon gamma production and diminishes interleukin 4 inhibition of such priming. *Proc Natl Acad Sci U S A* 1993;**90**:10188−92.
58. Takeda A, Hamano S, Yamanaka A, Hanada T, Ishibashi T, Mak TW, et al. Cutting edge: role of IL-27/WSX-1 signaling for induction of T-bet through activation of STAT1 during initial Th1 commitment. *J Immunol* 2003;**170**:4886−90.
59. van der Fits L, Mourits S, Voerman JSA, Kant M, Boon L, Laman JD, et al. Imiquimod-induced psoriasis-like skin inflammation in mice is mediated *via* the IL-23/IL-17 axis. *J Immunol* 2009;**182**:5836−45.
60. Hu X, Li J, Fu M, Zhao X, Wang W. The JAK/STAT signaling pathway: from bench to clinic. *Signal Transduct Target Ther* 2021;**6**:402.
61. Boehncke WH, Schön MP. Psoriasis. *Lancet* 2015;**386**:983−94.